



# Recent Advances in Supported Metal Catalysts and Oxide Catalysts for the Reverse Water-Gas Shift Reaction

Xiaodong Chen<sup>1,2,3†</sup>, Ya Chen<sup>4†</sup>, Chunyu Song<sup>1,2†</sup>, Peiyi Ji<sup>5</sup>, Nannan Wang<sup>1\*</sup>, Wenlong Wang<sup>1\*</sup> and Lifeng Cui<sup>1\*</sup>

## OPEN ACCESS

### Edited by:

Leilei Xu,  
Nanjing University of Information  
Science and Technology, China

### Reviewed by:

Miao Zhichao,  
Shandong University of  
Technology, China  
Bo Yang,  
Nanjing University of Information  
Science and Technology, China  
Mei Wu,  
Huaiyin Institute of Technology, China  
Qinghui Shou,  
Qingdao Institute of Bioenergy and  
Bioprocess Technology (CAS), China

### \*Correspondence:

Nannan Wang  
wangnn@dgut.edu.cn  
Wenlong Wang  
2016833@dgut.edu.cn  
Lifeng Cui  
lcui@dgut.edu.cn

<sup>†</sup>These authors have contributed  
equally to this work

### Specialty section:

This article was submitted to  
Catalysis and Photocatalysis,  
a section of the journal  
Frontiers in Chemistry

Received: 15 May 2020

Accepted: 09 July 2020

Published: 31 August 2020

### Citation:

Chen X, Chen Y, Song C, Ji P,  
Wang N, Wang W and Cui L (2020)  
Recent Advances in Supported Metal  
Catalysts and Oxide Catalysts for the  
Reverse Water-Gas Shift Reaction.  
Front. Chem. 8:709.  
doi: 10.3389/fchem.2020.00709

<sup>1</sup> School of Materials Science and Engineering, Dongguan University of Technology, Dongguan, China, <sup>2</sup> Center for Clean Energy Technology, Faculty of Science, School of Mathematical and Physical Science, University of Technology Sydney, Sydney, NSW, Australia, <sup>3</sup> Department of Applied Chemistry, School of Science, Xi'an Jiaotong University, Xi'an, China, <sup>4</sup> School of Physical Science and Technology, ShanghaiTech University, Shanghai, China, <sup>5</sup> College of Chemistry and Materials Science, Shanghai Normal University, Shanghai, China

The reverse water-gas shift reaction (RWGSR), a crucial stage in the conversion of abundant CO<sub>2</sub> into chemicals or hydrocarbon fuels, has attracted extensive attention as a renewable system to synthesize fuels by non-traditional routes. There have been persistent efforts to synthesize catalysts for industrial applications, with attention given to the catalytic activity, CO selectivity, and thermal stability. In this review, we describe the thermodynamics, kinetics, and atomic-level mechanisms of the RWGSR in relation to efficient RWGSR catalysts consisting of supported catalysts and oxide catalysts. In addition, we rationally classify, summarize, and analyze the effects of physicochemical properties, such as the morphologies, compositions, promoting abilities, and presence of strong metal-support interactions (SMSI), on the catalytic performance and CO selectivity in the RWGSR over supported catalysts. Regarding oxide catalysts (i.e., pure oxides, spinel, solid solution, and perovskite-type oxides), we emphasize the relationships among their surface structure, oxygen storage capacity (OSC), and catalytic performance in the RWGSR. Furthermore, the abilities of perovskite-type oxides to enhance the RWGSR with chemical looping cycles (RWGSR-CL) are systematically illustrated. These systematic introductions shed light on development of catalysts with high performance in RWGSR.

**Keywords:** RWGSR, catalytic mechanism, catalytic performance, supported metal catalysts, oxide catalysts, chemical looping cycles

## INTRODUCTION

The increasing emissions of anthropogenic CO<sub>2</sub> into our atmosphere through the unrestricted use of fossil fuels to drive industrial processes and human activity, particularly over the past few decades, has resulted in damage to the “carbon neutral” status of the earth and thus caused serious harm to the ecological system and to sustainable human development (Aresta et al., 2014). Therefore, the extensive efforts are needed to develop CO<sub>2</sub> utilization technologies to address these issues (Mikkelsen et al., 2010). Benefiting from plentiful low-cost CO<sub>2</sub> raw materials as well as the increasingly advanced CO<sub>2</sub> capture and separation technologies, CO<sub>2</sub> utilization is promising for commercial-scale applications (Aresta et al., 2016; Klankermayer et al., 2016).

The reverse water-gas shift reaction (RWGSR) is an indispensable part of CO<sub>2</sub> utilization because it is a non-fossil route for providing feedstock for important chemical processes, such as methanol synthesis (Gao et al., 2016; Huš et al., 2017), Fischer-Tropsch synthesis (Riedel et al., 1999), and Monsanto/Cativa acetic acid synthesis (Maitlis et al., 1996; Jones, 2000). When it is used as an intermediate step in the direct thermochemical transformation of CO<sub>2</sub> to hydrocarbons, such as methane (Sahebdehfar and Takht Ravanchi, 2015; Avanesian et al., 2016), ethanol (Sahebdehfar and Takht Ravanchi, 2015), low-carbon olefin (Liu et al., 2008; Zheng et al., 2017), and dimethyl ether (Centi and Perathoner, 2009), the RWGSR renders the process more practical. An important workable application of the RWGSR is associated with scarce H<sub>2</sub> reutilization in the Mars Exploration Program, in which it could regenerate H<sub>2</sub>O more easily for astronauts to utilize (Avanesian et al., 2016). In biomass-based solid oxide fuel cells, the ratio of CO<sub>2</sub>/CO/H<sub>2</sub> in the biomass gas can be considerably dictated by the RWGSR to realize its maximum energy storage efficiency (Chen et al., 2017a). Additionally, the RWGSR can be used to couple CO<sub>2</sub> with alkylene oxide or low alkanes to generate valuable chemicals, including ethylene glycol (Arunajatesan et al., 2001), styrene (Burri et al., 2007; Batista et al., 2010), and light olefins (Mukherjee et al., 2016; Kang et al., 2017). In contrast to the direct thermal cracking process, these coupled reactions can effortlessly break the thermodynamic equilibrium constraints and effectively accelerate their utilization (Reddy et al., 2008; Rao et al., 2009).

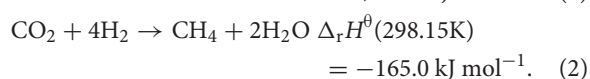
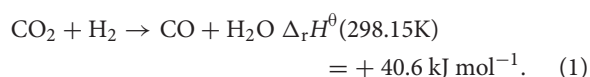
The chemically inert CO<sub>2</sub>, with its high C-O bond energy of 806 kJ mol<sup>-1</sup>, enables the chemical transformation of CO<sub>2</sub> to CO via the RWGSR (Wang et al., 2011). According to activation theory, the adsorption of CO<sub>2</sub> on the oxygen vacancy sites of certain catalysts initiates the first step of the RWGSR when it involves the cleavage of its own C-O bond under thermal energy-driven conditions (Su et al., 2019). There are two idiographic activation mechanisms proposed for the production of CO from the RWGSR based on experimental observations and theoretical calculations (Goguet et al., 2016). The first pathway is CO<sub>2</sub> hydrogenation to CO via the RWGSR, which proceeds via more reactive carboxyl (COOH\*) or formate (HCOO\*) intermediates, and the other pathway is the decomposition of CO<sub>2</sub> to CO\* + O\* via the direct C-O bond cleavage pathway (Weatherbee and Bartholomew, 1984; Kattel et al., 2016a). Once activated, these adsorbed intermediates will be instantaneously dissociated or desorbed on the constructed active centers of these catalysts to form the CO product (Tang et al., 2009; Roiaz et al., 2016). Based on this objective analysis, it is imperative to develop effective catalysts for CO<sub>2</sub> activation in the RWGSR.

In this review, we concentrate on the catalytic performance of the RWGSR with two major categories of heterogeneous catalysts, including supported metal catalysts and oxide catalysts, which is a subject of increasing interest. Utilizing the thermodynamics and kinetics analyses and the atomic-level mechanisms, the principles of RWGSR catalyst design will be comprehensively described. In addition, the physicochemical properties of supported catalysts, such as the morphologies,

compositions, promoting abilities, and presence of metal-support interactions, which affect the catalytic activity and CO selectivity of the RWGSR, will be systematically introduced to elucidate the structure-activity relationships. The relationships among the surface structure, oxygen storage capacity (OSC) and catalytic performance of oxide catalysts in the RWGSR are highlighted, especially for the application of perovskite-type oxides to enhance the RWGSR-CL. The present review provides general guidelines for the state-of-the-art architecture of heterogeneous catalysts for the RWGSR and a discussion of their challenges and further prospects.

## THERMODYNAMIC ANALYSIS

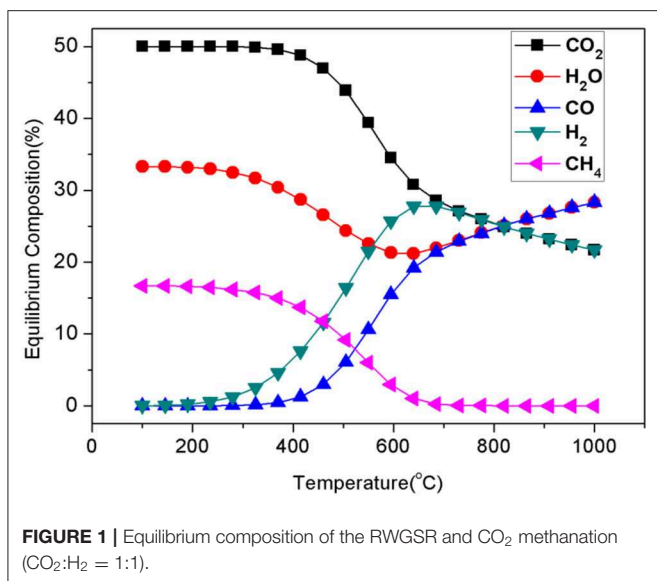
Since CO is arguably the most important C1-building block, the synthetic route of “CO<sub>2</sub>-to-CO” is considered an economical and valuable strategy (Barnard, 2008; Brennführer et al., 2009; Wu et al., 2011). Based on the thermodynamic standard enthalpy, the transformation of CO<sub>2</sub> to CO via the RWGSR is more thermodynamically favorable at elevated temperature because it is reversible and endothermic and because its chemical equilibrium is pressure independent, as shown in Equation (1). However, the RWGSR is always accompanied by undesired CO<sub>2</sub> methanation over the catalysts because of its excessive hydrogenation under ambient pressure (Kim et al., 2015; Ishito et al., 2016; Zhou et al., 2017). In addition, methanation is exothermic, favored at lower temperature, and pressure dependent, as shown in Equation (2).



For both the parallel and the cascade reactions over the catalysts, the CO yield is seriously restricted to H<sub>2</sub> utilization in additional competitive methanations. From the thermodynamic standpoint, as shown in **Figure 1**, the equilibrium composition favors the production of CH<sub>4</sub> rather than that of CO in the RWGSR at lower temperatures. Therefore, it is challenging to construct heterogeneous catalysts to restrict the production of undesirable CH<sub>4</sub> as a lower value-added by-product for applications at lower temperatures.

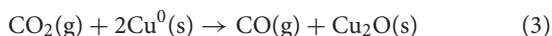
## MECHANISM

The well-known catalytic mechanisms proposed for the RWGSR reaction can be classified into two categories: surface redox mechanisms and associative mechanisms (Su et al., 2017). The major difference between these mechanisms is whether the dissociated H<sub>2</sub> species is involved in the formation of the carbon-containing intermediates, namely, formates, and carboxyls (Lin et al., 2017).

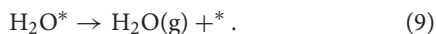
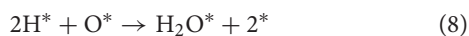
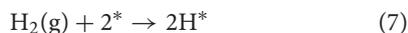
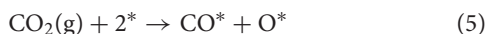


## Surface Redox Mechanism

The alternative oxido-reduction of active sites on the catalyst surface in the atmosphere of CO<sub>2</sub>/H<sub>2</sub> feedstock is believed to be a prerequisite for the sustainability of the RWGSR. For Cu-based catalysts, e.g., the reaction mechanism can be described as follows (Chen et al., 2000; Xu and Ge, 2016):



In these reactions, Cu<sup>0</sup>, the active site in the RWGSR, is involved in the rate-controlling step, CO<sub>2</sub> reduction. The CO<sub>2</sub> oxidizes the Cu<sup>0</sup> to generate Cu<sup>+</sup> and CO, while the H<sub>2</sub> reduces the Cu<sup>+</sup> to Cu<sup>0</sup> to form H<sub>2</sub>O; thus, the reaction conforms to a redox mechanism. When the whole catalytic process of the RWGSR is considered in detail, the mechanism of the surface redox reaction can be decomposed into the following basic steps (“\*” denotes the vacancy sites) (Gines et al., 1997; Fornero et al., 2017):

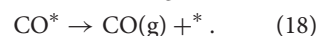
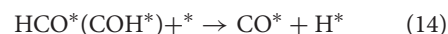


The study of kinetics is an important tool for establishing the redox mechanism of the RWGSR. Based on the Monte Carlo method to approximately simulate the RWGSR process over the Cu-based catalysts, CO<sub>2</sub> dissociates immediately to give CO and adsorbed oxygen species and is then reduced by H<sub>2</sub> with equivalent stoichiometric coefficients (Gines et al., 1997; Xu and Ge, 2016). In this process, the dissociative adsorption of CO<sub>2</sub> on the Cu particles is the rate-determining step, and the reduction of the adsorbed oxygen-containing species and surface

hydroxyls follows (Fujita et al., 1992; Wang et al., 2013b). Real-time temporal analysis of the products confirms that a surface-reduced Au/CeO<sub>2</sub> catalyst can be reoxidized by exposure to CO<sub>2</sub> pulses and that the surface oxygen deposited in this way can be reactively removed again, which is a prerequisite for the redox mechanism in the RWGSR. Furthermore, neglecting the changes in the hydroxyls and H<sub>2</sub>O on the surface imposed by the presence of H<sub>2</sub> in the feed, the activity for active oxygen deposition is sufficient to make the redox mechanism the dominant reaction pathway (Fornero et al., 2017). Realistically, the RWGSR proceeds through a redox mechanism over Au/TiO<sub>2</sub> catalysts in which the existing surface hydroxyls, surface Ti<sup>3+</sup>, and oxygen vacancies can jointly participate in the formation of a hydroxycarbonyl intermediate, which quickly decomposes to CO (Bobadilla et al., 2018). According to Density Functional Theory (DFT) calculations, the RWGSR on Cu@Mo<sub>2</sub>C (001) is preferentially selective for CO *via* a redox mechanism, and compared to the reaction *via* a COOH mechanism, the HCOO mechanism is kinetically less favorable due to its higher activation barrier in the rate-determining step, as shown in **Figure 2**. In the same way as the redox mechanism, the RWGSR occurs first by spontaneous dissociation of H<sub>2</sub> to form H\*, second by CO\* and O\* formation from the direct C-O bond cleavage of molecular CO<sub>2</sub>, third by the reaction of H\* and O\* to produce OH\*, fourth by the reaction of two OH\* species to generate H<sub>2</sub>O\*, and finally by the desorption of CO and H<sub>2</sub>O gas on the Cu@Mo<sub>2</sub>C (001) catalyst. Notably, the step for OH\* formation rather than CO\* formation in the redox mechanism, which has a higher activation barrier of 1.4 eV, is the rate-determining step (Jing et al., 2019).

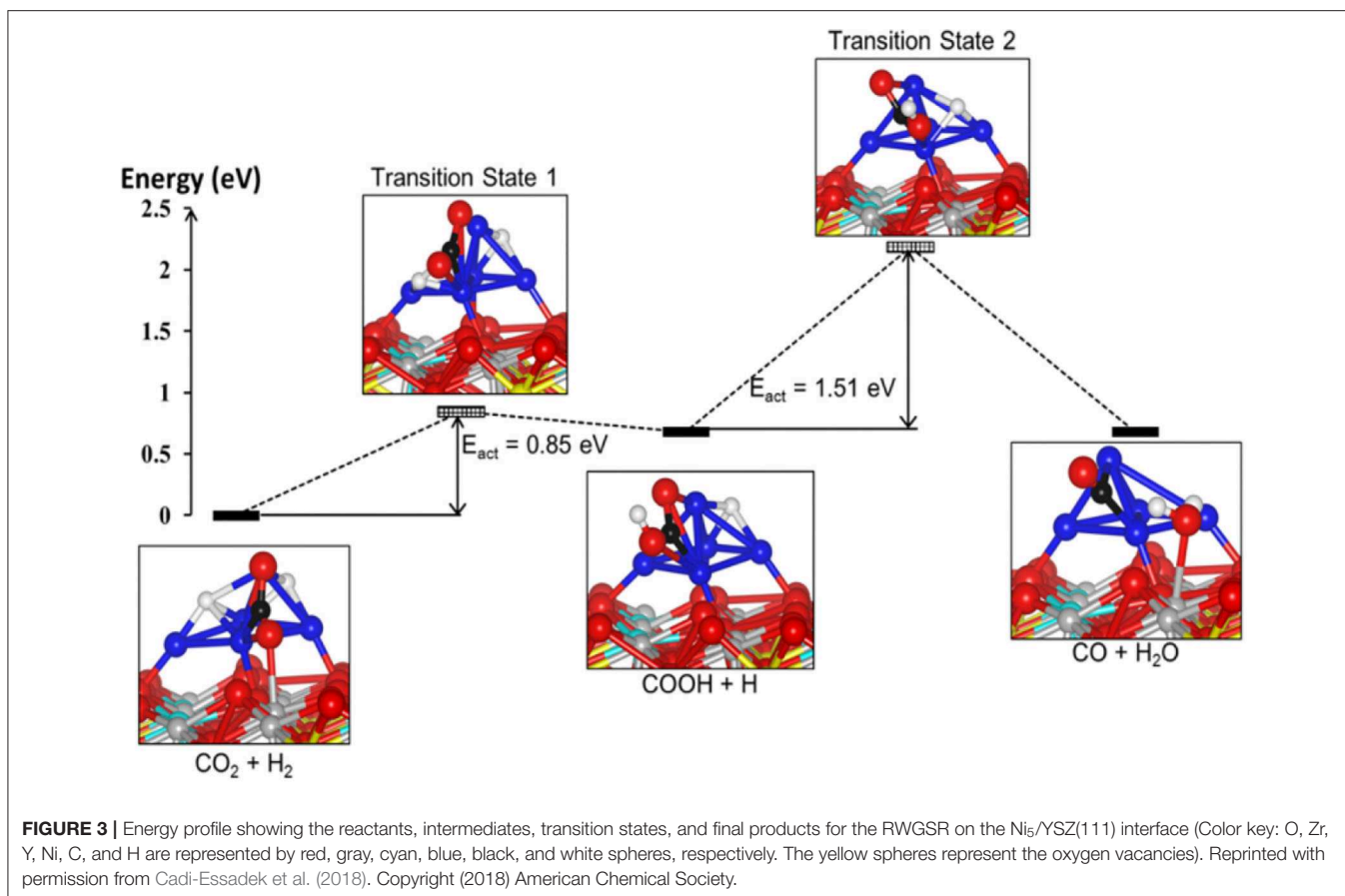
## Associative Mechanism Formate Species

The RWGSR pathway involves a formate (HCOO\*) intermediate that is formed by the initial CO<sub>2</sub>\* hydrogenation step and subsequently undergoes an instantaneous dissociation reaction to produce CO (Arunajatesan et al., 2007; Cao et al., 2016; Chen et al., 2016; Wolf et al., 2016). The reaction is described by the following steps (“\*” denotes the vacancy sites) (Chen et al., 2017a,b):

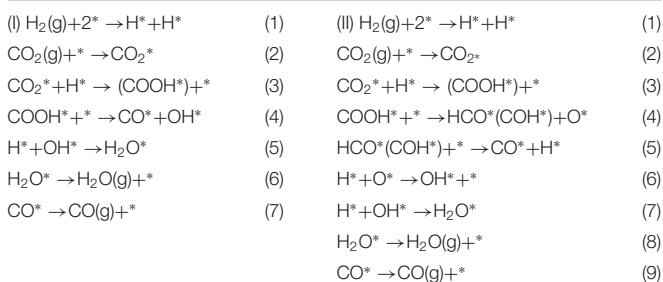


As indicated by the temperature-programmed desorption spectra of H<sub>2</sub>/CO<sub>2</sub> co-adsorbed on Cu/SiO<sub>2</sub> and Cu/K/SiO<sub>2</sub> catalysts, the H atoms either associate with CO<sub>2</sub>-Cu to form formates or





pathways, as shown below (“\*” denotes the vacancy sites) (Chen et al., 2017a,b).



On the basis of *in-situ* Fourier transform infrared spectroscopy (FT-IR) analyses, a Pt/TiO<sub>2</sub> catalyst treated at a high temperature and possessing reducible TiO<sub>2</sub> sites but no Pt sites is exclusively active for CO product, and thus the carboxyl species formed on the reducible TiO<sub>2</sub> sites are the intermediates in the formation of CO in the RWGSR (Kim et al., 2013). H/D isotopic substitution and kinetics and the results of the *in-situ* DRIFTS experiments illustrate that the CO formation proceeds *via* a mechanism in which H assists the dissociation of the C-O bond and that a carboxyl is a

more plausible intermediate than is a formate. In addition, the formates is still present on the Cu surface under the reaction conditions, but a fraction of them can be considered spectators of the reaction mechanism (Karelavic et al., 2019). The results from transient DRIFT-MS steady-state isotopic transient kinetic analysis analyses indicate that the characteristic exchange time (defined here as the time at which the DRIFTS signal of the intermediate decreases by 50% following the isotopic switch) of the carboxyl species agrees with that of the CO product (defined here as the time needed to achieve 50% exchange between the two isotopes, e.g., <sup>12</sup>CO(g) and <sup>13</sup>CO(g) of the main reaction product from MS measurements) when the feed gas is switched from <sup>13</sup>CO<sub>2</sub>/H<sub>2</sub> to <sup>12</sup>CO<sub>2</sub>/H<sub>2</sub> over the Pt/CeO<sub>2</sub> catalyst. These data quantitatively demonstrated that, for the present catalyst and conditions, the main reaction pathway is the formation of CO from the carboxyl species at the oxygen vacancies over the Pt-CeO<sub>x</sub> interface (Goguet et al., 2004a). DFT calculations indicate that the formation of COOH\* over Mo<sub>6</sub>S<sub>8</sub>-TM (TM = Pd, Pt, Ag) nanoclusters by the binding of the H\* atom to the O atom of CO<sub>2</sub>\* followed by its decomposition to CO is very favorable. Note that the COOH\* dissociation over Mo<sub>6</sub>S<sub>8</sub>-Ag is the rate-determining step in the overall process, whereas the rate-determining step of Mo<sub>6</sub>S<sub>8</sub>-Pd and Mo<sub>6</sub>S<sub>8</sub>-Pt in the carboxyl pathway is the transition step of the H<sub>2</sub> dissociation (Zheng et al., 2017). Moreover, DFT calculations show that the

RWGSR complies with a carboxyl mechanism over a Ni<sub>5</sub>/YSZ (111) catalyst through the identification of the structures and calculation of the energies of the intermediate state and two transition states, as shown in **Figure 3**. It has been suggested that one of the H\* atoms migrates toward the nearest O atom of the CO<sub>2</sub>\* to form the COOH\* intermediate and subsequently involves its protonation, allowing the formation of H<sub>2</sub>O\* adsorbed on the surface and the CO\* adsorbed on the Ni cluster. This calculation also shows that the second transition state for the dissociation of the COOH\* intermediate is the rate-determining step of the overall pathway and has an energy barrier of 1.51 eV (Cadi-Essadek et al., 2018).

## CATALYTIC SYSTEM

In recent decades, heterogeneous catalysts that promote the RWGSR have been extensively studied because of the gradual realization of their widespread application prospects for CO<sub>2</sub> utilization. At the early stage, much research has focused on the oxide catalysts due to their effluent oxygen vacancies sites, such as CeO<sub>2</sub>, CuO, ZnO, Al<sub>2</sub>O<sub>3</sub>, Fe<sub>2</sub>O<sub>3</sub>, Cr<sub>2</sub>O<sub>3</sub>, In<sub>2</sub>O<sub>3</sub>, and MnO<sub>2</sub> (Saeidi et al., 2017; Su et al., 2017; He et al., 2019). Although the CO selectivities of these oxide catalysts are desirable in RWGSR, their disadvantages of lower CO<sub>2</sub> activation and feasible poisons and sintering are hindering their extended application. In order to address these issues, persistent studies have concentrated on the fabrication of composite oxides (i.e., CuO/ZnO/Al<sub>2</sub>O<sub>3</sub>, NiO/CeO<sub>2</sub>, ZnO/Al<sub>2</sub>O<sub>3</sub>, ZnO/Cr<sub>2</sub>O<sub>3</sub>, CuOx/CeO<sub>2</sub>, CuO–CeO<sub>2</sub>/SBA-15, In<sub>2</sub>O<sub>3</sub>-CeO<sub>2</sub>, FeO<sub>x</sub>, etc.) (Liu et al., 2015; Dai et al., 2018; Ronda-Lloret et al., 2018; Panarities et al., 2020), spinel oxides (i.e., ZnAl<sub>2</sub>O<sub>4</sub>, ZnCr<sub>2</sub>O<sub>4</sub>, CuAl<sub>2</sub>O<sub>4</sub>, CoAl<sub>2</sub>O<sub>4</sub>, etc.) (Joo and Jung, 2003; Bahmanpour et al., 2019, 2020), solid solution oxides (i.e., Zn<sub>x</sub>Zr<sub>1-x</sub>O<sub>2-y</sub>, Ce<sub>0.5</sub>Zr<sub>0.5</sub>O<sub>2</sub>, Ni<sub>x</sub>Ce<sub>0.75</sub>Zr<sub>0.25-x</sub>O<sub>2</sub>, etc.) (Zonetti et al., 2014), and perovskite-type oxides (i.e., BaZr<sub>0.8</sub>Y<sub>0.16</sub>Zn<sub>0.04</sub>O<sub>3</sub>, La<sub>0.75</sub>Sr<sub>0.25</sub>CoO<sub>3-δ</sub>, La<sub>0.75</sub>Sr<sub>0.25</sub>FeO<sub>3</sub>, La<sub>0.75</sub>Sr<sub>0.25</sub>Fe<sub>1-y</sub>Cu<sub>y</sub>O<sub>3</sub>, LaNiO<sub>3</sub>, La<sub>0.9</sub>Sr<sub>0.1</sub>NiO<sub>3+δ</sub>, La<sub>0.9</sub>Sr<sub>0.1</sub>FeO<sub>3-δ</sub>, La<sub>0.9</sub>Sr<sub>0.1</sub>Ni<sub>0.5</sub>Fe<sub>0.5</sub>O<sub>3-δ</sub>, La<sub>0.75</sub>Sr<sub>0.25</sub>Cr<sub>0.5</sub>Mn<sub>0.5</sub>O<sub>3-δ</sub>, SrCe<sub>0.9</sub>Y<sub>0.1</sub>O<sub>3-δ</sub>, etc.) (Yamazoe et al., 1982; Ten Elshof et al., 1996; Klvana et al., 1999; Yang and Lin, 2006; Radovic et al., 2008; Zhuang et al., 2019; Bogolowski et al., 2020; Liu et al., 2020), which have the approvable characteristics of both stable structure and reverse oxygen storage capacity to increase RWGSR performance.

Recently, considerable efforts have been devoted to the design of metal-based catalysts (i.e., Pt, Pd, Au, Rh, Ru, Cu, Ni, Re, Co, Fe, Mo, etc.) immobilized onto the metal oxide support material (i.e., CeO<sub>2</sub>, TiO<sub>2</sub>, Al<sub>2</sub>O<sub>3</sub>, ZnO, ZrO<sub>2</sub>, SiO<sub>2</sub>, etc.) (Goguet et al., 2004b; Wang et al., 2011; Liu et al., 2015; Álvarez Galván et al., 2016; Ro et al., 2016; Nielsen et al., 2018) because they have metal/oxide interfaces with high reducibility to facilitate CO<sub>2</sub> activation in RWGSR. However, the CH<sub>4</sub> may be easily produced on these catalysts in the case of excessive hydrogenation of the C-O bond of the CO<sub>2</sub> molecule, which can be detrimental to CO selectivity (Yeung et al., 2005; Sun et al., 2015; Wang et al., 2016b; Kattel et al., 2017). In reality, an effective supported metal catalyst must be capable of both the C-O bond scission of CO<sub>2</sub>

and the appropriate hydrogenation. Thus, the supported metal catalysts must not only dissociate hydrogen relatively easily but also allow it to migrate onto the adjacent oxygen vacancies, where the adsorbed CO<sub>2</sub> is further hydrogenated (Chen and Cheng, 2002; Wang et al., 2017). Furthermore, the details of the activity and selectivity of some representative RWGSR catalysts under reaction conditions are presented in **Table 1**.

## Supported Metal Catalysts

The supported catalysts that can be seriously considered in the RWGSR due to their bifunctional catalytic roles for CO<sub>2</sub> activation and appropriate hydrogenation (Porosoff et al., 2016). However, RWGSR is demonstrated to be structure sensitive reaction; thus, the CO selectivity of which can be dictated by tailoring the structure functionality of supported catalysts through the SMSI effect, metal size effect, shape and crystal face effect, bimetallic effect, and alkali promoter effect to boost their concentrated activity.

### Strong Metal-Support Interaction (SMSI) Effect

The importance of support has been increasingly recognized in the decades following the discovery of SMSIs (Garin, 2001; Diebold, 2003; Neophytides et al., 2005; Fu and Wagner, 2007; Liu et al., 2013). In addition to dispersing metallic particles, the support also functions to influence the catalytic properties of the supported metal catalysts through geometric or electronic effects (Naito et al., 2006; Krstajić et al., 2008; Delgado et al., 2011; Li et al., 2015). In this section, the mechanisms by which SMSI effects provide catalytic characteristics of supported catalysts for the RWGSR are further elucidated.

The high electron donating property of metallic Pt in contact with a Ti<sup>3+</sup> ion site is caused by the SMSI effect, which generates new Pt-O<sub>v</sub>-Ti<sup>3+</sup> sites for CO production over the Pt/TiO<sub>2</sub> catalyst (Kim et al., 2012a,b, 2013). Additionally, by replacing the ZrO<sub>2</sub> support by TiO<sub>2</sub>, the SMSI effect selectively weakens the binding of the C-O bond and O-bond intermediates at the PtCo-oxide interface, thus leading to the high selectivity toward CO in the RWGSR (Kattel et al., 2016b). For TiO<sub>2</sub>-supported Rh catalysts, an adsorbate-mediated SMSI (A-SMSI) encapsulation state can be formed as a result of its treatment in a 20CO<sub>2</sub>:2H<sub>2</sub> environment at 250°C. The high coverage of the adsorbates (HCO<sub>x</sub>) on the support induces oxygen vacancy formation, driving the migration of the HCO<sub>x</sub>-functionalized support onto the metal. This A-SMSI encapsulation state is more stable against reoxidation by H<sub>2</sub>O in the RWGSR process compared with the SMSI encapsulation state formed as a result of only H<sub>2</sub> treatment, which modifies the reactivity of all the remaining exposed Rh sites and appears to be comprehensive in covering the Rh but permeable to reactants, due to its amorphous properties. Consequently, formation of the A-SMSI state induces a selectivity switch in the CO<sub>2</sub>-reduction reaction from the CH<sub>4</sub> production on the bare Rh particles to the CO product in the A-SMSI state, thus effectively rendering Rh less active for C-H bond formation (Matsubu et al., 2017). For Ir/CeO<sub>2</sub> catalysts, the SMSIs can enable more oxygen atoms to be incorporated

**TABLE 1** | Summary of the reaction conditions with conversion to and selectivity for CO, when available, for selected RWGSR catalysts.

Catalyst	Catalyst mass (mg)	H <sub>2</sub> /CO <sub>2</sub> ratio	WHSV (mL g <sub>cat</sub> <sup>-1</sup> h <sup>-1</sup> )	Temperature (°C)	Pressure (MPa)	Conversion (%)	Selectivity (%)
2%Pt/CeO <sub>2</sub> (Goguet et al., 2004b)	40	4:1	300,000	290	0.1	21.7	~100
1%Ni/CeO <sub>2</sub> (Wang et al., 2013a)	50	1:1	120,000	400	0.1	~4.5	~90
5%Ru/CeO <sub>2</sub> (Panaritis et al., 2018)	50	1:1	120,000	350	0.1	~16	~31
RuNi/CeZr (Sache et al., 2020)	250	4:1	24,000	350	0.1	53	93
FeNi/CeZr (Sache et al., 2020)	250	4:1	24,000	350	0.1	13	60
5%Ru/Sm-CeO <sub>2</sub> (Panaritis et al., 2018)	50	1:1	120,000	350	0.1	~16	~69
3.2%PtCo/CeO <sub>2</sub> (Kattel et al., 2016b)	N/A	2:1	N/A	300	0.1	9.1	92.3
PdNi/CeO <sub>2</sub> (Porosoff et al., 2014)	100	7:1	30,000	300	1.07 × 10 <sup>-4</sup>	2.5	37.5
10%Co/CeO <sub>2</sub> (Wang et al., 2013b)	20	3:1	300,000	300	0.1	3.8	39.4
1%Pt/TiO <sub>2</sub> (Kim et al., 2012b)	500	1:1	12,000	300	0.1	~13	~100
3.2%PtCo/TiO <sub>2</sub> (Kattel et al., 2016b)	N/A	2:1	N/A	300	0.1	8.2	98.8
0.2%Rh/TiO <sub>2</sub> (Matsubu et al., 2015)	15	4:1	40,000	200	0.1	N/A	~14.5
0.1%Ru/Al <sub>2</sub> O <sub>3</sub> (Matsubu et al., 2015)	50	3:1	720,000	400	0.1	~13	~80
1%Pt/Al <sub>2</sub> O <sub>3</sub> (Kim et al., 2012b)	500	1.43:1	12,000	300	0.1	~5.8	~100
Ni-Mo/Al <sub>2</sub> O <sub>3</sub> (Kharaji et al., 2014)	N/A	1:1	30,000	600	0.1	~35	N/A
Mo/Al <sub>2</sub> O <sub>3</sub> (Kharaji et al., 2014)	N/A	1:1	30,000	600	0.1	~15	N/A
Fe-Mo/γ-Al <sub>2</sub> O <sub>3</sub> (Kharaji et al., 2013)	5,000	1:1	N/A	400	0.1	~22	~100
Fe/γ-Al <sub>2</sub> O <sub>3</sub> (Kharaji et al., 2013)	5,000	1:1	N/A	400	0.1	~15.5	~100
PtCo/γ-Al <sub>2</sub> O <sub>3</sub> (Porosoff and Chen, 2013)	N/A	3:1	N/A	300	4 × 10 <sup>-3</sup>	10	89.4
20%Cu-Ni/γ-Al <sub>2</sub> O <sub>3</sub> (Liu and Liu, 1999)	N/A	1:1	2,000	500	0.1	23.2	75.5
3.2%PtCo/ZrO <sub>2</sub> (Kattel et al., 2016b)	N/A	2:1	N/A	300	0.1	7.8	89.5
0.5%Pd/La <sub>2</sub> O <sub>3</sub> /MWCNT (Kwak et al., 2013a)	50	3:1	72,000	400	0.1	~20	~100
0.5%Pd/MWCNT (Kwak et al., 2013a)	50	3:1	72,000	400	0.1	0	0
10%Cu-0.3%Fe/SiO <sub>2</sub> (Chen et al., 2004)	20	1:1	120,000	600	0.1	~12	~100
10%Cu/SiO <sub>2</sub> (Chen et al., 2004)	20	1:1	120,000	600	0.1	~8	~100
0.3%Fe/SiO <sub>2</sub> (Chen et al., 2004)	20	1:1	120,000	600	0.1	~2	~100
1%NiO/CeO <sub>2</sub> /SBA-15 (Lu and Kawamoto, 2014)	2,000	1:1	1,500	450	0.1	~2.5	100
ZnO/Al <sub>2</sub> O <sub>3</sub> (Zn:Al = 1:2) (Park et al., 2001)	N/A	3:1	15,000	400	0.1	~3.4	~100

(Continued)

TABLE 1 | Continued

Catalyst	Catalyst mass (mg)	H <sub>2</sub> /CO <sub>2</sub> ratio	WHSV (mL g <sub>cat</sub> <sup>-1</sup> h <sup>-1</sup> )	Temperature (°C)	Pressure (MPa)	Conversion (%)	Selectivity (%)
2D (δ)-MnO <sub>2</sub> (He et al., 2019)	30	1:1	40,000	850	0.1	50	100
ZnO (Park et al., 2001)	N/A	3:1	15,000	400	0.1	~2.6	~100
Al <sub>2</sub> O <sub>3</sub> (Park et al., 2001)	N/A	3:1	15,000	400	0.1	0	100
1%Cu/β-Mo <sub>2</sub> C (Zhang et al., 2016)	20	2:1	300,000	350	0.1	11	40
7.5%Co-Mo <sub>2</sub> C (Porosoff et al., 2014)	100	2:1	36,000	300	1.07 × 10 <sup>-4</sup>	9.5	~98.1
Mo <sub>2</sub> C (Porosoff et al., 2014)	100	2:1	36,000	300	1.07 × 10 <sup>-4</sup>	8.7	~93.5

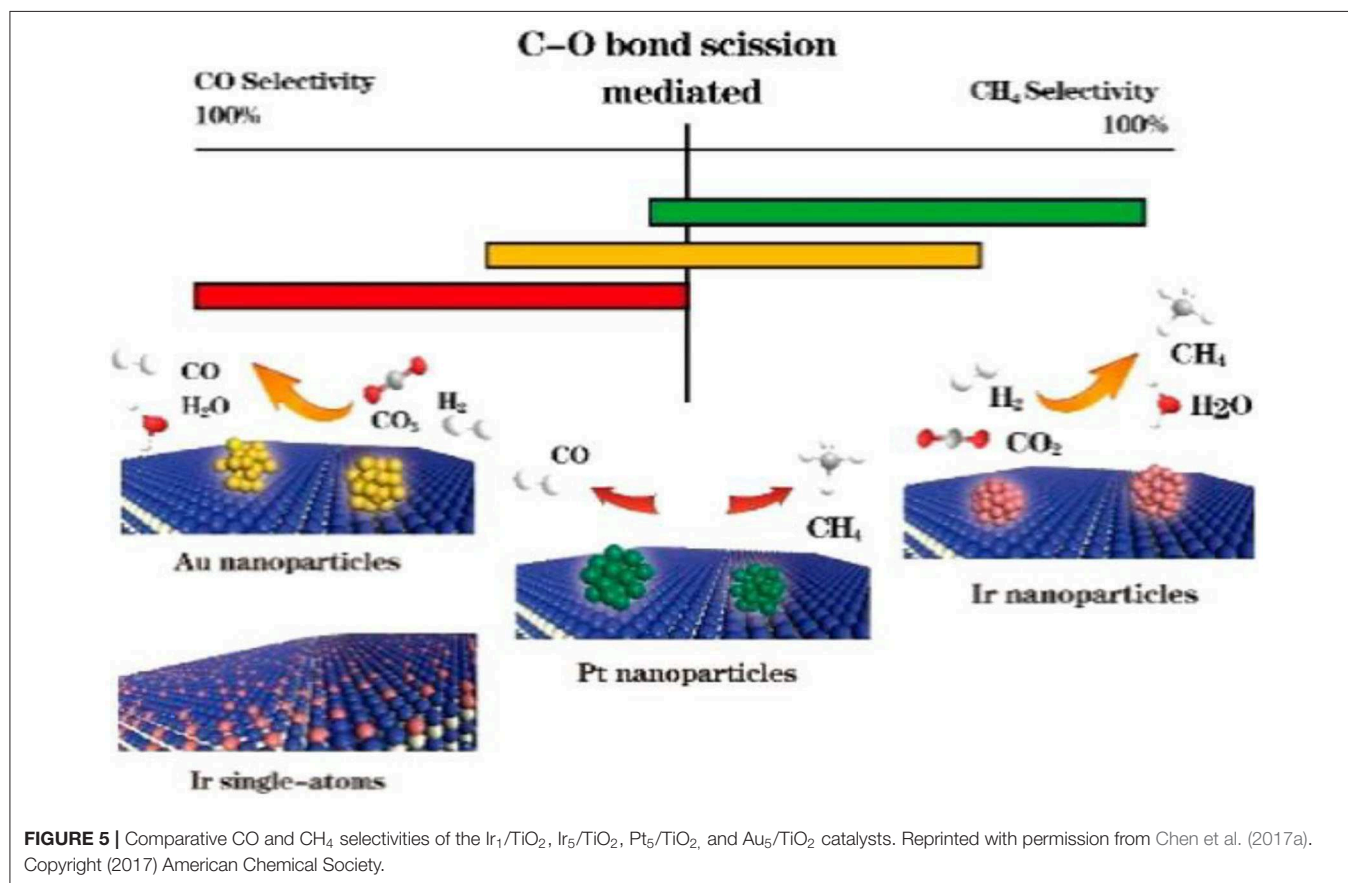
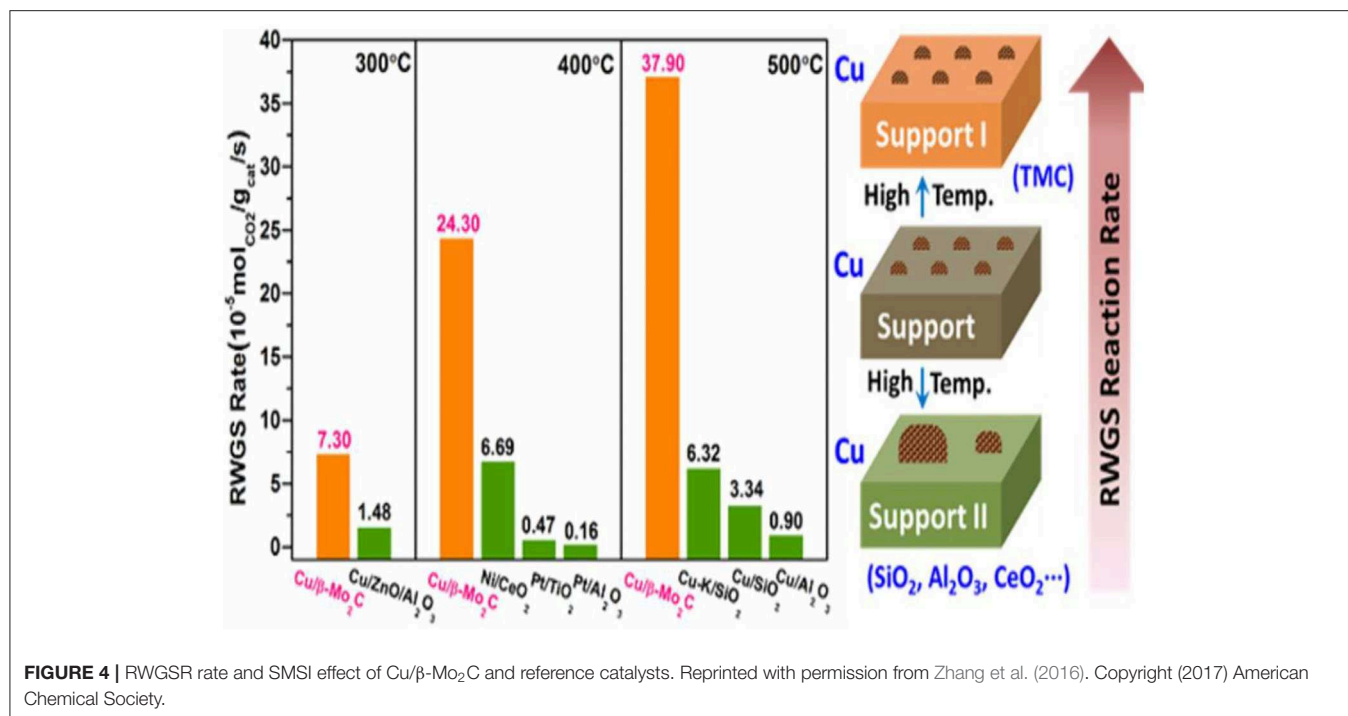
into the metal surface, resulting in a weaker CO adsorption strength over the partially oxidized Ir nanoparticles and giving a near 100% selectivity toward CO compared with that over the corresponding metallic Ir. Therefore, modulation of the chemical state of the metal species by the SMSI is more important for the regulation of the observed CO selectivity in the RWGSR (Li et al., 2017). For the Cu/CeO<sub>2</sub> catalyst, the Ce<sup>3+</sup>-O<sub>v</sub>-Cu<sup>0</sup> and Cu<sup>0</sup>-CeO<sub>2-δ</sub> interface structures can be generated by the electron transfer from Cu to Ce on its surface through SMSI effect, which can boost the adsorption and activation performance of reactant CO<sub>2</sub> and H<sub>2</sub> molecules for RWGSR (Zhou et al., 2020). In the simulation of catalytic CO<sub>2</sub> reduction by Pd-decorated silicon-hydride nanosheets (Pd@SiNS), the direct SMSI between the Pd nanoparticle and the Si nanosheet causes H transfer from the Pd to the oxidized SiNS surface, which may occur repeatedly by two mechanisms. First, an H atom adsorbed on the Pd nanoparticle interacts with a surface Si-O-Si and creates a Si-OH; second, another H from the Pd nanoparticle forms a bond with the Si-OH, which leads to desorption of the H<sub>2</sub>O, creating a surface radical, thereby enabling a catalytic cycle. Furthermore, the strain induced in the SiNS by the Si-O-Si bonds enhances the reactivity of the oxidized SiNS surface toward the transformation of CO<sub>2</sub> to CO under mild conditions (Qian et al., 2019). In the context of Mo<sub>2</sub>C-supported Co catalysts, the SMSI effect facilitates the formation of the amorphous CoMoC<sub>y</sub>O<sub>z</sub> phase formed during the CO<sub>2</sub> hydrogenation, in which the Co with a positive charge is identified as the critical active site that dissociates CH<sub>4</sub> to CO. Therefore, the addition of 7.5% Co to Mo<sub>2</sub>C leads to an increase in conversion from 8.7 to 9.5%, while the CO:CH<sub>4</sub> ratio increases from 15 to 51 (Porosoff et al., 2014). When Cu is added to the β-Mo<sub>2</sub>C support during the preparation process, the SMSI effect not only promotes the dispersion of supported copper and prevents the aggregation of Cu particles but also enables a portion of the electrons to transfer from Cu to Mo<sub>2</sub>C so that the Cu<sup>+</sup> and Cu<sup>0</sup> species coexist in the Cu/β-Mo<sub>2</sub>C catalyst. Its modulated electronic structure makes the highly dispersed Cu species more active in the CO<sub>2</sub> activation and accelerates the CO\* desorption in the following transformation reactions, which accounts for its excellent activity in the RWGSR, as depicted in **Figure 4** (Zhang et al., 2016).

### Metal Size Effect

The RWGSR is considered structure sensitive for supported catalysts, of which the intermediate dissociation pathway associated with H assistance is substantially dependent on the size of the anchored metal active sites and thus exerts an influence on the CO selectivity of the RWGSR (Chen et al., 2017a).

Multiple studies have been conducted to study the size effect of metal sites relative to CO selectivity in supported noble metal catalysts. The metal active sites (i.e., Pt, Pd, Ru) dispersed at an atomic level contribute more to the CO product compared to metal clusters at a 3D level. This phenomenon is a consequence of the absence of larger metals clusters in which the initially formed CO<sub>ad</sub> can be further activated during the continuous reaction (Kwak et al., 2013a,b; Wang et al., 2016a; Chen et al., 2017a). In addition, the Pd sites that slightly retain the CO surface species formed from the formates and other intermediates are more prevalent on the surface of the smaller Pd particles and thus exhibit a higher selectivity toward the CO product. In contrast, the larger Pd particles, due to a higher population of terrace sites in which it is easier to form multi-bound CO and dissociated H<sub>2</sub> bound in the vicinity of CO, reveal a stronger interaction with CO. These stable CO species are mainly in multi-bound forms and act as the direct intermediates to CH<sub>4</sub> (Wang et al., 2015, 2017). Matsubu et al. have utilized DRIFTS with known site-specific extinction coefficients to quantify the fraction of Rh sites residing as atomically dispersed isolated sites (Rh<sub>iso</sub>), as well as Rh sites on the surface of Rh nanoparticles (Rh<sub>NP</sub>) for a series of TiO<sub>2</sub> supported Rh catalysts. The reaction condition-induced disintegration of Rh<sub>NP</sub>, which form the Rh<sub>iso</sub> active sites, have been observed to control the CO selectivity of the RWGSR (Matsubu et al., 2015). Furthermore, we have determined that the difference between the desorption energy and dissociation barrier of metal carbonyls is a critical factor for determining the CO selectivity of the RWGSR by combining DFT calculations and experiments, as shown in **Figure 5**. Specifically, narrowing the size of the Ir active sites by decreasing the Ir loading over Ir/TiO<sub>2</sub> catalysts can hinder the carbonyl dissociation but improve the CO desorption, giving rise to CO selectivity (Chen et al., 2017a).

For supported non-noble metal catalysts, significant efforts on Ni-based catalysts have also shown that smaller anchored Ni active sites are beneficial to produce CO in the RWGSR



(Wang et al., 2013a,d; Lu and Kawamoto, 2014). The consecutive pathway is favored on small Ni particles, which is attributed to low H<sub>2</sub> coverage on the Ni surface, thus leading to the dissociation of the intermediates and high CO selectivity. Whereas the RWGSR on large Ni particles may be controlled by mixed consecutive and parallel pathways, it increases the likelihood that the intermediates will be competitively hydrogenated to CO or CH<sub>4</sub> as part of a parallel reaction pathway (Wu et al., 2015). Millet et al. reported on the activation of CO<sub>2</sub> on Ni single-atom catalysts that are synthesized using a solid solution approach by controlled substitution of 1–10 atom % of Mg<sup>2+</sup> by Ni<sup>2+</sup> inside the MgO structure. The Ni atoms are preferentially located on the surface of the MgO and, as predicted by hybrid-functional calculations, favor the low-coordinated sites, where they can reduce the strength of the CO<sub>2</sub> binding and promote H<sub>2</sub> dissociation. Thus, the Ni atoms are active for CO<sub>2</sub> conversion through the RWGSR but are unable to conduct its further hydrogenation to CH<sub>4</sub>, for which Ni clusters are needed (Millet et al., 2019).

### Shape and Crystal Face Effect

RWGSR activities are also significantly depending on the shape and exposed crystal face of catalysts because they can determine the virtual adsorption energy and desorption energy of intermediates in the reaction process (Liu et al., 2019).

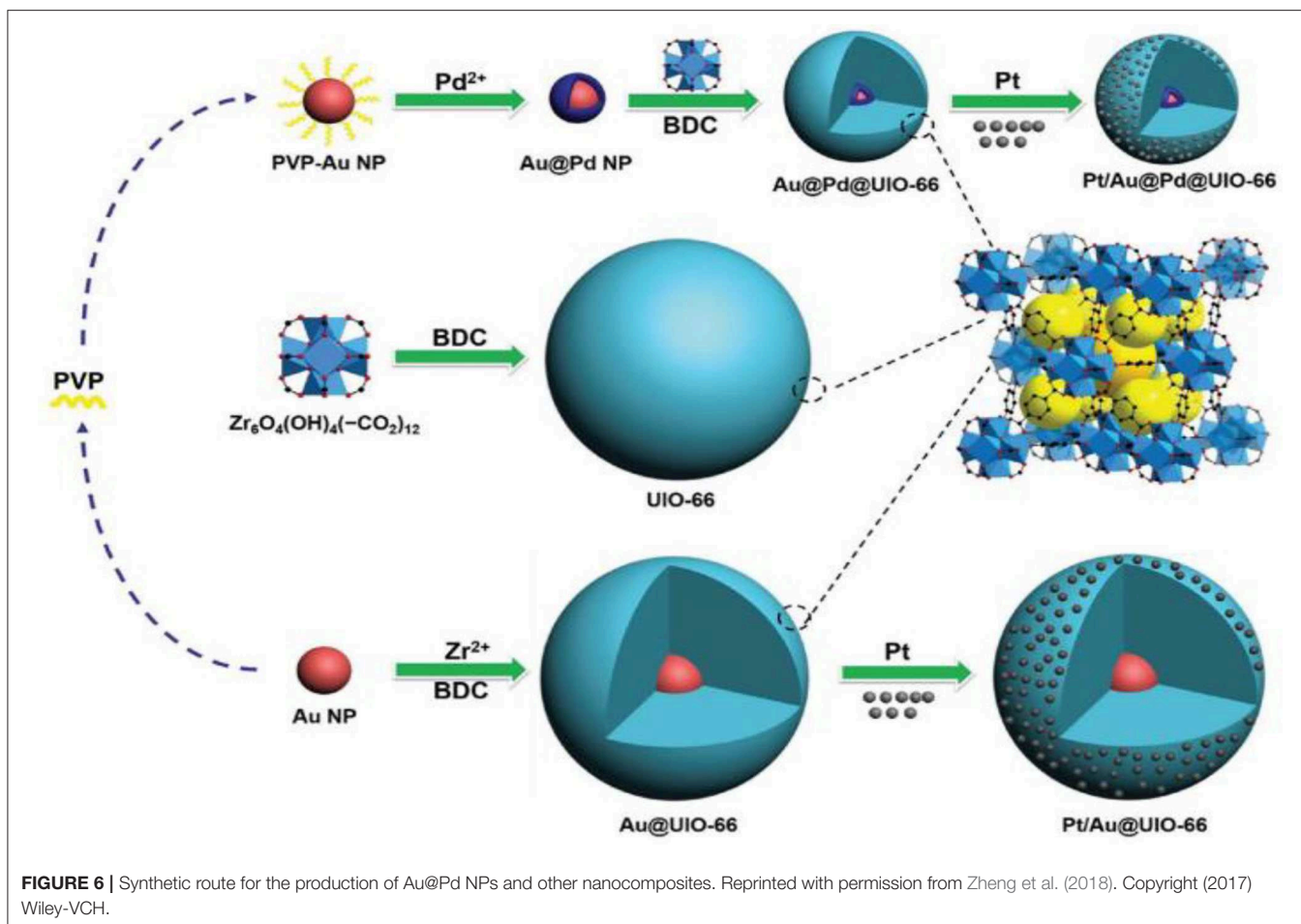
Up to now, abundant efforts have been dedicated to study the effect of surface structure of Cu-based catalysts on RWGSR performance. Through the simulation of the adsorption of CO<sub>2</sub>, H<sub>2</sub>, H, O, OH, CO, and H<sub>2</sub>O on the Cu(*hkl*) surfaces at low coverage, it has been demonstrated that the trend in the calculated activation barriers for the reaction is CO<sub>2</sub> dissociative adsorption (namely CO<sub>2,g</sub> COs + Os) follows the order of Cu(110) < Cu(100) < Cu(111), suggesting that the most efficient crystal surface for catalyzing RWGSR by copper is Cu(110), and the more densely packed Cu(111) surface is the least active among the Cu(*hkl*) surfaces studied here (Nakamura et al., 1998; Wang et al., 2003; Wang and Nakamura, 2010). When the Cu particles are doped onto the CeO<sub>2</sub>-Nanorod and CeO<sub>2</sub>-Nanosphere surfaces, respectively, which can be marked as Cu/CeO<sub>2</sub>-NR(111) and Cu/CeO<sub>2</sub>-NS(110), by comparison, the Cu/CeO<sub>2</sub>-NR displays the higher RWGSR activity. This is mainly because that the CO<sub>2</sub> dissociative activation and the formation of active bidentate carbonate and formate intermediates over CeO<sub>2</sub>(110) become more feasible (Kovacevic et al., 2016; Lin et al., 2018b). Furthermore, self-assembled CeO<sub>2</sub> with 3D hollow nanosphere, nanoparticle, and nanocube morphologies are used to support Cu particles, which can be denoted as Cu/CeO<sub>2</sub>-hs(111), Cu/CeO<sub>2</sub>-np(111), and Cu/CeO<sub>2</sub>-nc(200), respectively. Thereinto, the Cu/CeO<sub>2</sub>-hs(111) presents the best catalytic RWGSR performance among these as-prepared catalysts due to its high concentration of active oxygen vacancies sites (Zhang et al., 2020). For PtCo/TiO<sub>2</sub>(110), \*HCOO is formed as an intermediate, which may eventually produce CO, whereas for PtCo/CeO<sub>2</sub>(110), the aside from the route that proceeds *via* \*HCOO, a pathway *via* a \*CH<sub>3</sub>O intermediate is operating in parallel, which likely leads to the formation of CH<sub>4</sub>. Moreover, DFT calculation demonstrates that the adsorption of CO<sub>2</sub> is

stronger at the Ni<sub>n</sub>/YSZ(111) ( $n = 4-7, 10, \text{ and } 20$ ) interface than on the clean YSZ(111) between the Ni clusters and the YSZ(111) surface, which facilitates the transformation of CO<sub>2</sub> to CO (Cadi-Essadek et al., 2018). For Cu@Mo<sub>2</sub>C(001) and Cu<sub>4</sub>@Mo<sub>2</sub>C(001) surfaces, although the dissociative adsorption of H<sub>2</sub> on these two surface is barrier-free and highly exothermic, the activation barrier of carboxyl formation or C-O bond scission as a rate-limiting step on the Cu<sub>4</sub>@Mo<sub>2</sub>C(001) surfaces is smaller, and the desorption of CO at the Cu site needs less heat than Mo site, thereby accelerating CO<sub>2</sub> conversion in RWGSR (Chen and Cheng, 2002).

### Bimetallic Effect

The behavior of a catalyst is modulated by its interaction with other catalyst components, such as a second metal, which influences it through electronic interactions, generates interfacial active sites, or is directly involved in the reaction by bonding to reactants or intermediates (Liu and Liu, 1999; Liu et al., 2015). Therefore, supported bimetallic catalysts have been extensively used for the RWGSR due to their tuning catalytic activity that may be achieved by two metals working synergistically.

The existence of Mo in the structure of the Fe-Mo/Al<sub>2</sub>O<sub>3</sub> catalyst enhances its catalytic performance for the RWGSR due to the electronic effect, which transfers electrons from Fe to Mo and leads to an electron-deficient state of the Fe species, in which it is not helpful for CO adsorption and hence inhibits the continuous hydrogenation of the intermediates (Kharaji et al., 2013; Panaritis et al., 2018). It is reasonable for the Ni species with the electron deficient state to possess high catalytic performance for RWGSR when Ni is added as a second metal component to the Mo/Al<sub>2</sub>O<sub>3</sub> catalyst (Kharaji et al., 2014). As for RuNi/CeZr catalyst, the addition of Ru enhances the Ni reducibility and leads to greater Ni dispersion on the catalyst surface, thus promoting overall activity and CO selectivity for the RWGSR (Sache et al., 2020). Typically, MOF-74 plays a role in helping adsorb and deliver electrons, whereas the low amount of Au@Pd NPs in Au@Pd@MOF-74 results in the poor photon adsorption strength of the Au@Pd active sites. Based on this feature, the core-shell Au@Pd@MOF-74 nanostructure is more propitious to generate CO than MOF-74 in the RWGSR because CO generation is a two-electron reaction, while CH<sub>4</sub> generation requires eight electrons; thus, it is more difficult to produce CH<sub>4</sub> (Han et al., 2019). Because of the functional characteristics of Au@Pd nanoparticles, the Pt/Au@Pd@UIO-66 catalyst is synthesized to improve its catalytic activity in the RWGSR, as shown in **Figure 6**. In this system, the core-shell monodispersed Au@Pd nanosphere is encapsulated in the UIO-66 to control its morphology and impart nanoparticle functionality. Additionally, the microporous nature of the UIO-66 assists the adsorption of the Pt nanoparticles, which enhances the interaction between them, favoring the formation of isolated and well-dispersed Pt nanoparticle active sites. This advanced architecture results in excellent catalytic activity and CO selectivity for the RWGSR, and the concept of inserting nanoparticles into microporous MOFs will revolutionize future industrial applications (Zheng et al., 2018). DFT calculations



indicate that the catalytic behavior of a  $\text{Cu}_{12}\text{TM}$  ( $\text{TM} = \text{Co}, \text{Rh}, \text{Ir}, \text{Ni}, \text{Pd}, \text{Ag}, \text{Au}$ ) bimetallic nanocluster in the RWGSR is dependent on the position of the d-band center. In general, the closer the d-band center is to the Fermi level of these catalysts, the greater is the  $\text{CO}_2$  adsorption energy, and the smaller is the C-O bond dissociation barrier. Therefore,  $\text{Cu}_{12}\text{Co}$  delivers better catalytic activity for the RWGSR, with a TOF value of  $8.96 \times 10^{-13} \text{ s}^{-1}$ , than do the  $\text{Cu}_{13}$  and  $\text{Cu}_{12}\text{TM}$  bimetallic systems, due to its d-center value of  $-0.547 \text{ eV}$ , which is higher than that of the other two systems (Zhang and Guo, 2018). Furthermore, for  $\gamma\text{-Al}_2\text{O}_3$ - and  $\text{CeO}_2$ -supported Co catalysts, with the addition of Pt as the second component, the values of the d-band center move from the Fermi level toward more negative values, which prevents the excessive hydrogenation of the C-O bond of the  $\text{CO}_2$  molecule and thereby increases the CO selectivity of the RWGSR (Porosoff and Chen, 2013). In addition, the deposition of Mo onto Au/ $\text{SiO}_2$  catalyst generates new Au/ $\text{MoO}_x$  interfacial sites since it preferentially occurs on undercoordinated Au sites. The heat of CO adsorption ( $\Delta H_{\text{ads}}$ ) for the Au/ $\text{MoO}_x$  sites is  $33 \text{ kJ mol}^{-1}$ , considerably lower than that of the  $\text{Au}^0$  sites, indicating that these interfacial sites are more selective than the  $\text{Au}^0$  sites for the RWGSR (Carrasquillo-Flores et al., 2015). Similarly, the Cu/Fe interfacial

active sites are generated after introduction of additional Fe into the Cu/ $\text{SiO}_2$  catalyst, on which the formation of the Fe-Cu bond also prevents Cu from being sintered and oxidized during the RWGSR (Chen et al., 2004). Moreover, the addition of Cu to the Mo/FAU catalyst results in an improvement in the reducibility of  $\text{MoO}_3$ . Therefore, the  $\text{Mo}(0.8)\text{Cu}(0.2)/\text{FAU}$  catalyst, which contains co-supported Mo-Cu at an atomic ratio of 4:1, exhibits the higher CO yield of 18.5% and selectivity of 99% compared with the supported Mo catalyst for the RWGSR with the feed gas ( $\text{H}_2:\text{CO}_2 = 1:1$ ) at atmosphere pressure and 773K (Okemoto et al., 2020). The bulk  $\text{Pt}_3\text{Ni}$  intermetallic parent compound is formed selectively over the Pt-Ni bimetallic catalysts supported on mesoporous silica, which is related to the thermodynamics of the phase equilibria with a metal silicate that precludes the formation of more Ni-rich intermetallics during the operando conditions of the RWGSR, as shown in Figure 7. This proposed intermetallic structure for these  $\sim 1 \text{ nm}$  supported clusters, shows a surface/interfacial speciation of the Ni in which only heterometallic Pt-Ni interactions are present in an atomic arrangement within the catalytically active bimetallic sites, which afford exceptionally high activity and CO selectivity in the RWGSR (Liu et al., 2018).

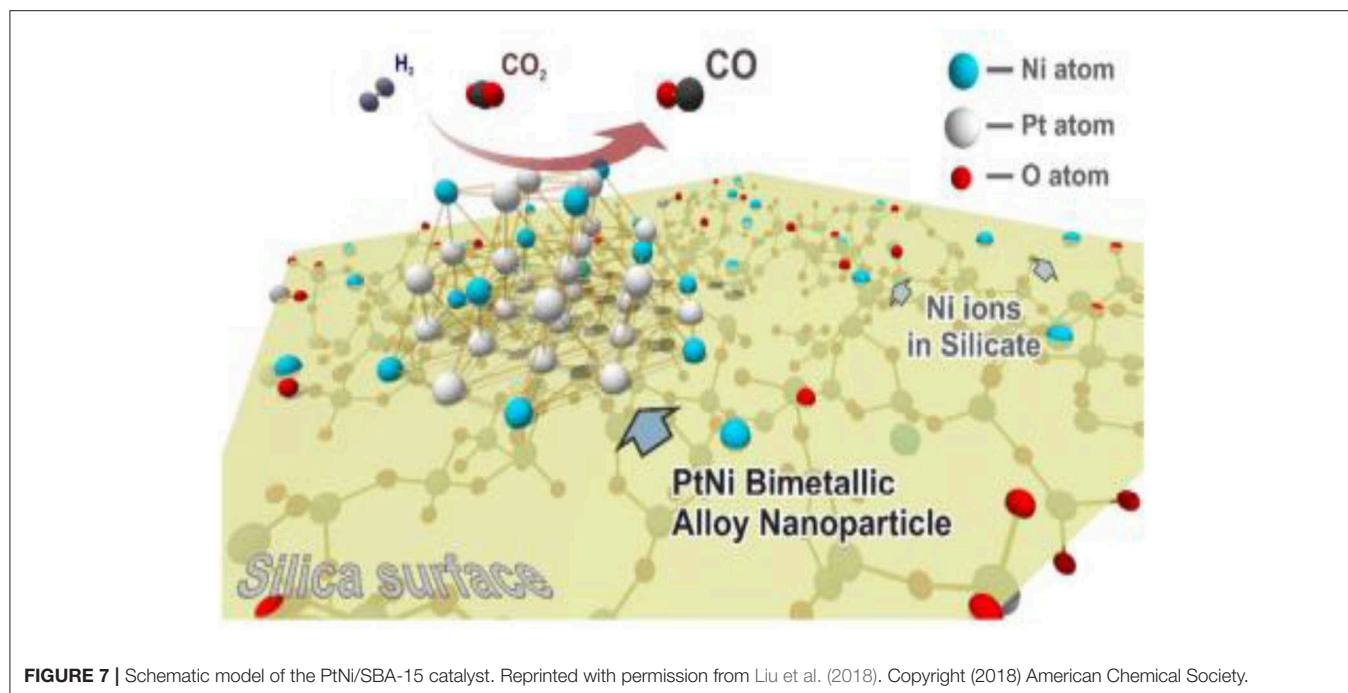


**FIGURE 7** | Schematic model of the PtNi/SBA-15 catalyst. Reprinted with permission from Liu et al. (2018). Copyright (2018) American Chemical Society.

### Alkali Promoter Effect

For supported heterogeneous catalysts, alkali metal components are typically introduced as promoters to increase the amount of adsorption sites and mediate the adsorption strength of the reactants and intermediates on the “inert support” (Li et al., 1998; Gálvez et al., 2013; Obalová et al., 2013; Connor and Holland, 2017; Pacultová et al., 2017). For instance, the addition of alkali metal promoters is crucial for industrial catalysts substantially applied in the Fisher-Tropsch synthesis (Mirzaei et al., 2006; Okabe et al., 2007; Feyzi et al., 2011; Cosultchi et al., 2012) and ammonia synthesis (Shimoda et al., 2017; Lin et al., 2018; Jafari et al., 2019; Rogowski, 2019; Zhou et al., 2019). In the field of RWGSRs, abundant studies have shown that K and other promoter additives are essential for some supported catalysts to acquire the expected CO product (Arunajatesan et al., 2007).

The highly K-promoted Fe/Al<sub>2</sub>O<sub>3</sub> and Cu/SiO<sub>2</sub> catalysts give much higher CO formation rates than do their counterparts in the RWGSR mainly because the addition of K introduces abundant weak, medium, and strong basic sites, which helps to adsorb/activate CO<sub>2</sub> and further converts the CO<sub>2</sub> to CO through reaction (Choi et al., 1996; Chen et al., 2003). For the Ni/Al<sub>2</sub>O<sub>3</sub> catalyst, carbonates are the main intermediates, decomposition of which to CO is relatively difficult. However, *via* modification of this catalyst with a strong base such KOH, the formates rather than the carbonate forms as the main intermediate, which strongly absorbs on the surface of the Ni-KOH/Al<sub>2</sub>O<sub>3</sub> catalyst, contributes to CO formation and hinders further hydrogenation of the CO to CH<sub>4</sub> through C-O bond scission (Zhang et al., 2019a). Furthermore, it is demonstrated that the introduction of alkali promoter (K, Mg) by co-impregnation technique enhance the dispersity of Ni active species on the Al<sub>2</sub>O<sub>3</sub>, thus increasing the RWGSR performance (Ranjabar et al., 2019). The addition of

K promoter leads to an electron transfer from Pt to O in KO<sub>x</sub> species, resulting in the generation of interfacial active sites over the Pt/mutite catalyst, which is proposed to be more responsible for the production of CO (Liang et al., 2017). Similarly, the K promoter acts as a reducing agent relative to the Fe metal, and the observed increase in the ratio of the Fe<sup>2+</sup>/Fe<sup>3+</sup> ions over the BaFe-hexaaluminates after the K addition reflects the increasing concentration of reduced Fe<sup>2+</sup> ions in the hexaaluminate lattice, which is accompanied by the appearance of oxygen vacancies due to the cleavage of one of the neighboring Fe-O-M (M = Al, Ba) bonds in the first coordination sphere of Fe ions. These vacancies play a role in the sites for CO<sub>2</sub> adsorption forming monodentate surface carbonates followed by redox transformation evolving CO and leaving the second oxygen bonded to the Fe<sup>3+</sup> ion (Wang et al., 2013b,c; Utsis et al., 2018). The results of DFT calculations demonstrate that the K adatom greatly stabilizes the adsorption of all oxygenate intermediates through direct K-O bonding formation on K-modified Cu(111) and Cu(110) surfaces, thus promoting CO<sub>2</sub> dissociation in the RWGSR. In general, the different promoting effects of alkali metals on CO<sub>2</sub> dissociation are due to their electronegativities, which induce different work function changes and surface dipole moments. Correspondingly, the promoting effects on CO<sub>2</sub> dissociation induced by alkali metals increase in the order of Na < K < Rb < Cs, while the electronegativity of various alkali metals decreases in the order of Na > K > Rb > Cs (Wang and Wang, 2019). In accordance with the above effects, the electronegative character facilitates the electronic transfer from Cs to Mo and Fe and leads to an electronically rich surface, which favors the selectivity toward CO over the corresponding catalysts (Pastor-Pérez et al., 2018; Zhang et al., 2019b). For the WC/ $\gamma$ -Al<sub>2</sub>O<sub>3</sub> catalyst, the addition of the K promoter not only has a structural effect

to promote the dispersion of the WC species across the high surface area support but also can serve as electronic promotion to strengthen CO and CO<sub>2</sub> adsorption while weakening H<sub>2</sub> adsorption, which is therefore hypothesized to result in a lower H<sub>2</sub>/Co<sub>x</sub> on the catalyst surface, thus inhibiting hydrogenation activity for CH<sub>4</sub> and accelerating the generation of CO *via* the RWGSR (Morse et al., 2020). Specifically, our studies have systematically investigated the effect of K promoter on the activities and selectivities of zeolite L-supported Pt catalysts for the RWGSR, as shown in **Figure 8**. This study concluded that an additive K promoter not only alters the work function of Pt through their interaction but also forms Pt-O(OH)-K interfacial sites. In addition, the electronic properties of Pt-O(OH)-K sites, with a charge transfer from the Pt surface to the adjacent O in KO<sub>x</sub>, facilitate the formation of formate intermediates and desorption of the CO. However, with excessive addition of K, the access of the reactants to the Pt surface and interface is tightly blocked. Thus, the activity of the RWGSR is significantly promoted by the controlled addition of K promoter (Yang et al., 2017).

### Oxide Catalysts

Reducible transition oxides are intensively employed in RWGSR catalysts due to their relative abundance and their OSC, which is the ability to reversibly store and release oxygen while formally switching the valence state of the metal ion in its own structure under a CO<sub>2</sub>/H<sub>2</sub> atmosphere (Reddy et al., 2010; Dong et al., 2012; Yao et al., 2013). The O atom can be deprived of H<sub>2</sub> in the oxide lattice to generate surface oxygen vacancies, which are much more favorable to the generation of CO rather than CH<sub>4</sub>, because the oxygen from the C-O bond cleavage of the CO<sub>2</sub> molecule can be accommodated, but this leads to unsatisfactory catalytic activity and thermal stability (Katta et al., 2010; Ahn et al., 2012; Graciani et al., 2014). Normally, the additional introduction of heteroatoms into the oxides leads to the formation of spinel, solid solution, and perovskite-type oxides, and their ultra-stable structure is conducive to reversible oxygen donor-acceptor over oxygen vacancies sites, which thus effectively overcome the disadvantages of pure oxides as RWGSR catalysts (Ringuedé and Fouletier, 2001; Royer et al., 2005).

ZnO-based oxides are preferentially utilized to catalyze the RWGSR during the CAMARE process due to its ease of formation of metal composite oxides with high stability and specific activity (Li et al., 2002; Schmale et al., 2013). Nonetheless, ZnO-based oxide catalysts are vulnerable to the reduction of ZnO to Zn metal and therefore the loss of ZnO active components when exposed to high thermal reaction conditions, which contributes to their catalytic deactivation (Park et al., 2001). The formation of the spinel structure of the ZnAl<sub>2</sub>O<sub>4</sub> phase by addition of Al<sub>2</sub>O<sub>3</sub> to the ZnO catalyst can cause resistance to its catalytic deactivation in the RWGSR (Joo and Jung, 2003). Similarly, when Fe<sub>2</sub>O<sub>3</sub> is substituted by ZnO over the Fe<sub>2</sub>O<sub>3</sub>/Cr<sub>2</sub>O<sub>3</sub> catalyst, the corresponding ZnCr<sub>2</sub>O<sub>4</sub> phase is formed and thus becomes stable (Park et al., 2000). In the synthetic process of the ZnZrO<sub>x</sub> mixed oxide, the substitution of the Zr in the first layers of the *m*-ZrO<sub>2</sub> lattice with Zn causes the formation of a surface solution (Zn<sub>x</sub>Zr<sub>1-x</sub>O<sub>2-y</sub>), which generates

oxygen vacancies and improves its stability, reducibility, and oxygen mobility, thus increasing the CO<sub>2</sub> conversion in the RWGSR (Silva-Calpa et al., 2016).

The widespread application of CeO<sub>2</sub>-based oxide in RWGSR catalysts is mainly due to its high OSC, which is inextricably correlated with the catalytic activity (Masui et al., 1997; Wang and Liu, 2018). Both the manipulation of the CeO<sub>2</sub> shape with emphasis on tuning its fraction of reactive crystal planes and the doping CeO<sub>2</sub> with heterocations to alter its structure and chemical properties are effective strategies to obtain a superior OSC (Sun et al., 2012; Zhou and Li, 2012). Considering their distinct morphologies (particles, rods, and cubes), the higher activity of CeO<sub>2</sub> cubes in the RWGSR is due to the superior inherent reactivity of the CeO<sub>2</sub> (100) crystal planes enclosing the cubes, contrary to the less inherently reactive CeO<sub>2</sub> (111) facets enclosing the rods and particles in the RWGSR (Kovacevic et al., 2016). The CeO<sub>2</sub> lattice distortion caused by the incorporation of heterocations such as Zn increases the oxygen vacancy defects and thus accelerates the mobility of the oxygen ions, leading to a higher OSC, thus markedly enhancing its catalytic activity in the RWGSR (Lin et al., 2015; Wenzel et al., 2017). In addition, either Ce<sub>0.75</sub>Zr<sub>0.25</sub>O<sub>2</sub> or Ce<sub>0.75</sub>Zr<sub>0.5</sub>O<sub>2</sub> solid solution can be formed by the addition of Zr to the CeO<sub>2</sub> lattice, increasing its ability to generate oxygen vacancies and, more importantly, promoting its thermal stability, which is a very promising aspect of catalytic systems employed in reactions in which the RWGSR is one of the steps in the processes that generate hydrocarbons from CO<sub>2</sub> (Zonetti et al., 2014; Wenzel et al., 2018).

The adsorption of CO<sub>2</sub> on In<sub>2</sub>O<sub>3</sub> has an adsorption energy of -1.25 eV, which is sufficiently exothermic and thus favorable, so the O-C-O angle of the CO<sub>2</sub> on adsorbed on the In<sub>2</sub>O<sub>3</sub> is significantly distorted relative to the gas phase structure, significantly increasing the activity of the CO<sub>2</sub> in the RWGSR (Ye et al., 2012; Sun et al., 2014). The oxygen vacancies are increasingly created and stabilized on In<sub>2</sub>O<sub>3</sub> with the presence of CeO<sub>2</sub> in the In<sub>2</sub>O<sub>3</sub>-CeO<sub>2</sub> catalyst, on which the dissociated H<sub>2</sub> adsorption is enhanced and the amount of bicarbonate species resulting from activated CO<sub>2</sub> is increased, which thus exhibits enhanced catalytic activity for the RWGSR (Wang et al., 2016c). Cubic In<sub>2</sub>O<sub>3</sub>[denoted as *c*-In<sub>2</sub>O<sub>3</sub>(110)] exhibits a higher RWGSR rate than the hexagonal In<sub>2</sub>O<sub>3</sub>[denoted as *h*-In<sub>2</sub>O<sub>3</sub>(110)] at temperature below 350°C due to its enhanced dissociative adsorption of H<sub>2</sub>, facile formation of the oxygen vacancies, and enhanced ability to adsorb and activate CO<sub>2</sub> on the oxygen vacancies (Wang et al., 2020). DFT calculations indicate that the oxygen vacancies sites on the In<sub>2</sub>O<sub>3</sub> (110) surface assist CO<sub>2</sub> activation and hydrogenation and stabilize the key intermediates involved in CO formation (Ye et al., 2013). Furthermore, an In<sub>2</sub>O<sub>3-x</sub>(OH)<sub>y</sub> surface containing both Lewis base hydroxide groups and Lewis acid In sites together with oxygen vacancies can heterolytically dissociate H<sub>2</sub> to form a hydride bonded to In metal and a proton bonded to a lattice O. This hydrogenated In<sub>2</sub>O<sub>3-x</sub>(OH)<sub>y</sub> surface facilitates CO<sub>2</sub> reduction by mediating the charge transfer between the In<sub>2</sub>O<sub>3-x</sub>(OH)<sub>y</sub> surface and adsorbed reactants CO<sub>2</sub> and H<sub>2</sub> to form CO and H<sub>2</sub>O (Ghuman et al., 2015). Well-tempered MetaD-biased AIMD simulations have been performed, taking

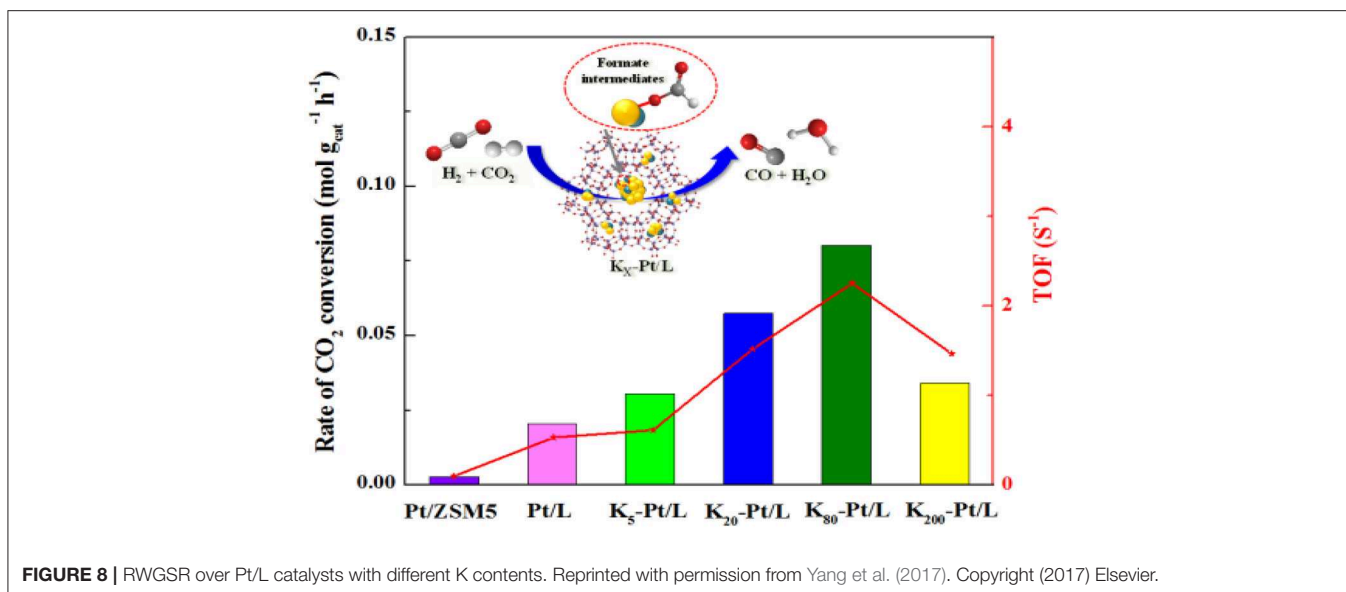


**FIGURE 8** | RWGSR over Pt/L catalysts with different K contents. Reprinted with permission from Yang et al. (2017). Copyright (2017) Elsevier.

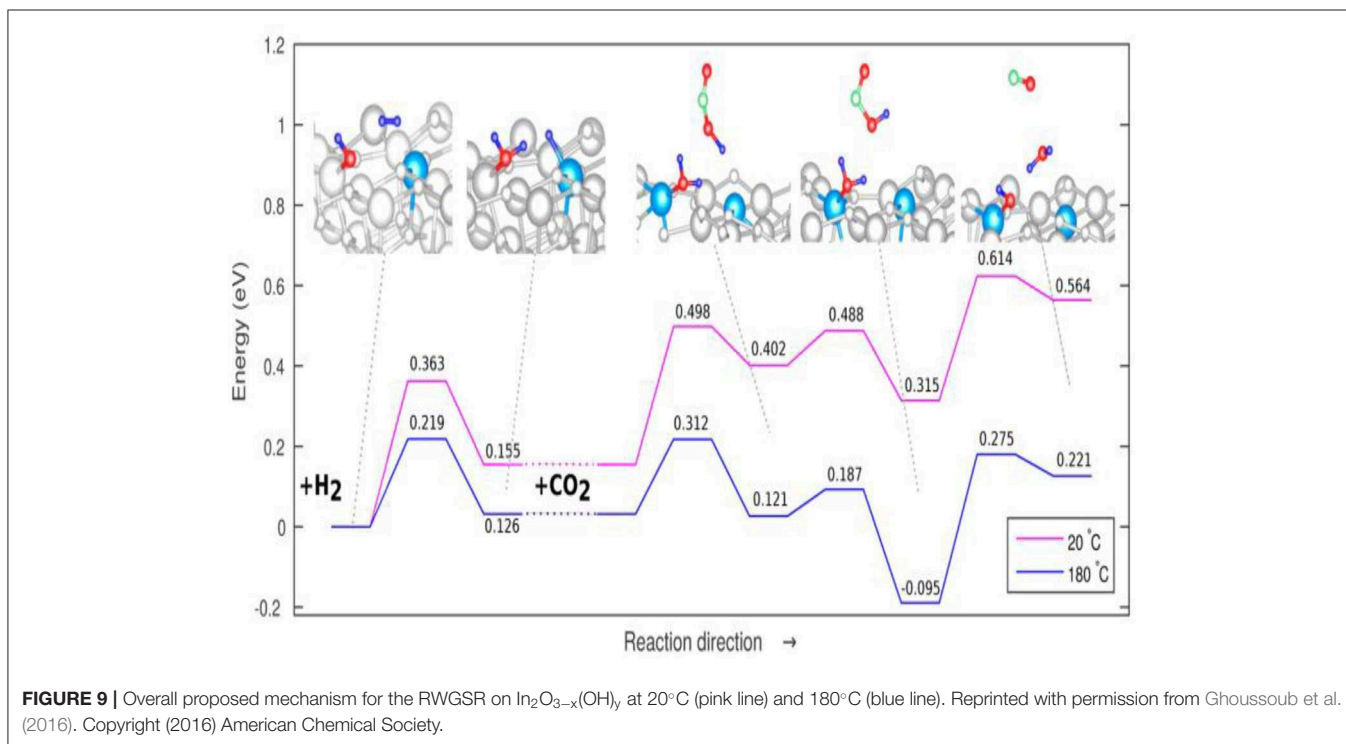


**FIGURE 9** | Overall proposed mechanism for the RWGSR on In<sub>2</sub>O<sub>3-x</sub>(OH)<sub>y</sub> at 20°C (pink line) and 180°C (blue line). Reprinted with permission from Ghossoub et al. (2016). Copyright (2016) American Chemical Society.

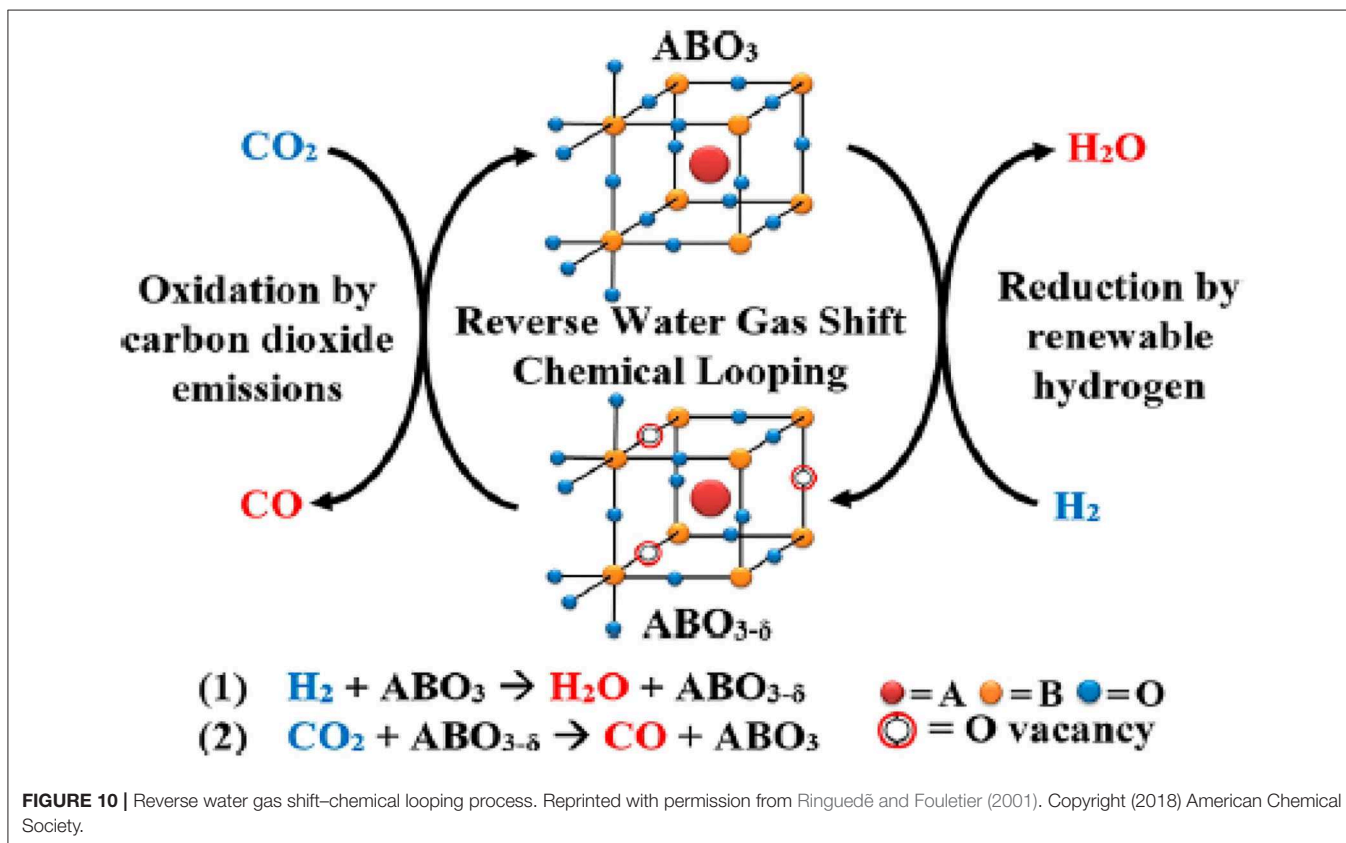
the temperature into account, to probe the mechanism for the RWGSR reaction over the In<sub>2</sub>O<sub>3-x</sub>(OH)<sub>y</sub> surface at temperatures of 20 and 180°C, as shown in **Figure 9**, and the results show that the reduction of gaseous CO<sub>2</sub> is the rate-limiting step, with no significant change resulting from increased temperature. However, the energy barrier corresponding to the adsorption of CO<sub>2</sub> is slightly reduced at 180°C compared to the that at 20°C, suggesting that the thermal effects may only be relevant to the reaction step characterized by an adsorptive mechanisms and that the increased thermal conditions may enhance the reactivity

by enabling the surface frustrated Lewis pairs to become further spatially separated (Ghossoub et al., 2016).

The perovskite-type oxides are represented by an ABO<sub>3</sub> formula, where the A-site is typically occupied by lanthanides or alkaline earth metals, and the B-site is usually filled with transition metals (Yamazoe et al., 1981; Peña and Fierro, 2001; de Lima et al., 2009). With multiple cation combinations possible on each site, perovskite-type oxides can be easily customized to achieve desirable properties, such as high oxygen mobility and tunability, together with thermal stability at high temperatures

without aggregation (Royer et al., 2005; Kae et al., 2014). Therefore, these materials are attractive for application to the RWGSR with chemical looping cycles (RWGSR-CL) that can convert  $\text{CO}_2$  and  $\text{H}_2$  to separate streams of  $\text{CO}$  and  $\text{H}_2\text{O}$ , as depicted in **Figure 10** (Ringuedé and Fouletier, 2001). The combination of La and Sr in the A-site and metal in the B-site enhances the formation of oxygen vacancies due to the generation of a charge imbalance in the  $\text{ABO}_3$  structure caused by the difference in their oxidation states (Daza et al., 2014). Regarding Co-based perovskite type oxides ( $\text{La}_{0.75}\text{Sr}_{0.25}\text{CoO}_{3-\delta}$ ), under  $\text{H}_2$  flow conditions, their phases can change to metallic cobalt and base oxides ( $\text{Co/SrCO}_3/\text{La}_2\text{O}_3$ ), which are then reoxidized to a layered perovskite ( $\text{CoO/LaSrCoO}_{4-\delta}$ ) with a  $\text{K}_2\text{NiF}_4$ -type structure when exposed to  $\text{CO}_2$ , thus producing  $\text{CO}$  during this cycle. Additionally, the optimal isothermal reduction and conversion temperatures for maximizing the  $\text{CO}$  product rates of  $113.9 \mu\text{mole CO/g/min}$  are  $500^\circ\text{C}$  (of  $400, 500, \text{ and } 600^\circ\text{C}$ ) and  $850^\circ\text{C}$  (of  $650, 750, \text{ and } 850^\circ\text{C}$ ), presumably due to the formation of mixed oxides and metallic cobalt crystalline phases (observed via X-ray diffraction) in close contact under these conditions (Royer et al., 2005). Fe-based perovskite type oxides [ $\text{La}_{0.75}\text{Sr}_{0.25}\text{FeO}_3$  (LSF)] have shown the greatest promise in the RWGSR-CL process due to the low energy barrier for oxidation-state transitions ( $\text{Fe}^{3+}\text{-Fe}^{2+}$ ) during the redox cycles (Peña and Fierro, 2001). Enhanced oxygen self-diffusion, material recyclability, and therefore the viability of LSF have been demonstrated for chemical looping

when supported by redox materials with more abundant alternatives, such as  $\text{CeO}_2$ ,  $\text{ZrO}_2$ ,  $\text{Al}_2\text{O}_3$ ,  $\text{SiO}_2$ , and  $\text{TiO}_2$  (Li et al., 2011; Chen et al., 2014). In comparison, supports such as  $\text{TiO}_2$  and  $\text{Al}_2\text{O}_3$  demonstrate SMSIs, which often result in some degree of LSF particle encapsulation, even at low temperatures, thus hindering the  $\text{CO}_2$  adsorption on the surface oxygen vacancies, whereas  $\text{SiO}_2$  demonstrates more moderate interactions that are strong enough and suitable for particle segregation yet weak enough to avoid deactivation (Min et al., 2003; Hare et al., 2019). These behaviors occur because the utilization of  $\text{SiO}_2$  as a support significantly reduces the average LSF crystallite size and the extent of oxygen self-diffusion retardation, and the  $\text{CO}$  generation yields of LSF/ $\text{SiO}_2$  surpass those of LSF alone by  $\sim 200\%$ , producing  $2.6 \text{ mmol of CO}_{\text{gLSF}}^{-1}$  at a peak rate of  $0.8 \text{ mmol CO}_{\text{gLSF}}^{-1} \text{ min}^{-1}$  (Hare et al., 2018). In addition, further modification of Fe-based perovskite type oxides with transition metals helps to increase the strength of the interaction of the active species and support and thus stabilizes the unusual cationic oxidation state in the RWGSR process (Nitarori et al., 1988). The incorporation of Cu in  $\text{La}_{0.75}\text{Sr}_{0.25}\text{Fe}_{1-Y}\text{Cu}_Y\text{O}_3$  perovskites [ $\text{Cu}100^*Y$  (with  $Y = 0, 0.10, 0.25, 0.50, 0.75, \text{ and } 1$ )] facilitates the formation of oxygen vacancies at lower temperatures.  $\text{CO}$  production is promoted in the Cu10 sample vs. Cu0 and Cu25, likely due to a combined effect of better  $\text{CO}_2$  dissociative chemisorption energies on metallic Cu and decreased thermodynamic stability of the oxygen-deficient perovskites



(Daza et al., 2016). The enhanced crystalline structure stability is aroused by the incorporation of Co in the  $\text{La}_{0.75}\text{Sr}_{0.25}\text{Co}_{(1-Y)}\text{Fe}_Y\text{O}_3$  perovskite. Additionally, a computational investigation using DFT calculations correlates  $\text{CO}_2$  adsorption strength, generally a strong barrier in  $\text{CO}_2$  conversion, on the (100) crystal facets on  $\text{La}_{0.75}\text{Sr}_{0.25}\text{FeO}_{(3-\delta)}$  to increasing the surface oxygen vacancies ( $\delta$ ). Therefore,  $\delta$  in the perovskite is the driving force to break the CO-O bond and reoxidize the  $\text{La}_{0.75}\text{Sr}_{0.25}\text{FeO}_{3-\delta}$  (Daza et al., 2015; Maiti et al., 2016).

## CONCLUSION AND OUTLOOK

The large-scale conversion of  $\text{CO}_2$  to CO *via* the RWGSR is a promising route with great potential for use in the near future, provided a mature technology for commercial production of renewable  $\text{H}_2$  is also available. The RWGSR also achieves higher  $\text{CO}_2$  conversion than other relevant technologies that meet the global  $\text{CO}_2$  emissions standards. Because it is a slightly endothermic and pressure-independent reaction, the current challenge for RWGSR employed in fuel synthesis is the design of thermally stable materials that can achieve high CO selectivity and high production rates. Preferential strategies have recently been enacted to address the existing problems either by modulating the SMSI, size of the active metal, second metal composition, and addition of alkali promoter for supported catalysts or by dipping with additional heteroatoms or tuning their crystal planes for oxide catalysts. Furthermore, the perovskite-type oxides can act as the oxygen donor-acceptor for the RWGSR-CL to not only circumvent thermodynamic and kinetic limitations but also eliminate the possibility of methanation as a side reaction because there is no direct interaction between two feed gases and between two product streams.

From this systematic introduction, the relationships between the nature of the active sites and the main intermediates of RWGSR catalysts are understood through the insights gained

from the molecular dynamic simulations and mechanistic work under the operando reaction conditions, which is beneficial to the development of state-of-the-art architecture of RWGSR catalysts. However, even though several materials have been studied, improvements are still possible, especially for commercial development of RWGSR catalysts for laboratory and market applications. If the RWGSR plays a major role in the reduction of the atmospheric  $\text{CO}_2$  concentration, then designing catalysts with earth-abundant materials will be necessary and desirable. To develop supported metals, both Fe oxides and Ni oxides are chosen to be investigated as representative substitutes for the most commonly used reducible supports, such as  $\text{CeO}_2$ , ZnO, and  $\text{In}_2\text{O}_3$ , largely due to their oxygen vacancies with high oxygen mobility and stability, which can activate  $\text{CO}_2$  more easily by accommodating oxygen due to the C-O bond cleavage in the RWGSR. Additionally, transition metal carbides are attractive and convenient alternatives for industrial use in the RWGSR because of their properties, which are similar to those of precious metals, as well as their dual functionality for  $\text{H}_2$  dissociation and C-O bond scission and their potential to behave similarly to reducible oxides.

## AUTHOR CONTRIBUTIONS

XC, CS, and YC drafted the manuscript, conceived the concept of the review, conducted literature survey, and arranged the figures. NW provided the suggestions. WW and LC revised the manuscript and provided comments. All authors contributed to the article and approved the submitted version.

## FUNDING

This project is financially supported by the Startup Research Fund of Dongguan University of Technology (KCYKYQD2017015), the Postdoctoral Startup Research Fund of Dongguan University of Technology (No.196100040019), and the China Postdoctoral Science Foundation (No. 2019M653608).

## REFERENCES

- Ahn, K. Y., Yoo, D. S., Prasad, D. H., Lee, H. W., Chung, Y. C., and Lee, J. H. (2012). Role of multivalent Pr in the formation and migration of oxygen vacancy in Pr-Doped ceria: experimental and first-principles investigations. *Chem. Mater.* 24, 4261–4267. doi: 10.1021/cm3022424
- Álvarez Galván, C., Schumann, J., Behrens, M., Fieero, J. L. G., Schlögl, R., and Frei, E. (2016). Reverse water-gas shift reaction at the Cu/ZnO interface: influence of the Cu/Zn ratio on structure-activity correlations. *Appl. Catal. B-Environ.* 195, 104–111. doi: 10.1016/j.apcatb.2016.05.007
- Aresta, M., Dibenedetto, A., and Angelini, A. (2014). Catalysis for the valorization of exhaust carbon: from  $\text{CO}_2$  to chemicals, materials, and fuels technological use of  $\text{CO}_2$ . *Chem. Rev.* 114, 1709–1742. doi: 10.1021/cr4002758
- Aresta, M., Dibenedetto, A., and Quaranta, E. (2016). State of the art and perspectives in catalytic processes for  $\text{CO}_2$  conversion into chemicals and fuels: the distinctive contribution of chemical catalysis and biotechnology. *J. Catal.* 343, 2–45. doi: 10.1016/j.jcat.2016.04.003
- Arunajatesan, V., Subramaniam, B., Hutchenson, K. W., and Herkes, F. E. (2001). Fixed-bed hydrogenation of organic compounds in supercritical carbon dioxide. *Chem. Eng. Sci.* 56, 1363–1369. doi: 10.1016/S0009-2509(00)0359-6
- Arunajatesan, V., Subramaniam, B., Hutchenson, K. W., and Herkes, F. E. (2007). *In situ* FTIR investigations of reverse water gas shift reaction activity at supercritical conditions. *Chem. Eng. Sci.* 62, 5062–5069. doi: 10.1016/j.ces.2007.01.010
- Avanesian, T., Gusmão, G. S., and Christopher, P. (2016). Mechanism of  $\text{CO}_2$  reduction by  $\text{H}_2$  on Ru(0001) and general selectivity descriptors for late-transition metal catalysts. *J. Catal.* 343, 86–96. doi: 10.1016/j.jcat.2016.03.016
- Bahmanpour, A. M., Héroguel, F., Kiliç M., Baranowski, C. J., Artiglia, L., Röthlisberger, U., et al. (2019). Cu-Al spinel as a highly active and stable catalyst for the reverse water gas shift reaction. *ACS Catal.* 9, 6243–6251. doi: 10.1021/acscatal.9b01822
- Bahmanpour, A. M., Héroguel, F., Kiliç M., Baranowski, C. J., Schouwink, P., and Röthlisberger, U. (2020). Essential role of oxygen vacancies of Cu-Al and Co-Al spinel oxides in their activity for the reverse water gas shift reaction. *Appl. Catal. B-Environ.* 266:118669. doi: 10.1016/j.apcatb.2020.118669
- Barnard, C. F. J. (2008). Palladium-catalyzed carbonylation -a reaction come of age. *Organometallics* 27, 5402–5422. doi: 10.1021/om800549q

- Batista, A. H. M., Ramos, F. S. O., Braga, T. P., Lima, C. L., de Sousa, F. F., de Barros, E. B., et al. (2010). Mesoporous  $\text{MAl}_2\text{O}_4$  (M=Cu, Ni, Fe or Mg) spinels: characterisation and application in the catalytic dehydrogenation of ethylbenzene in the presence of  $\text{CO}_2$ . *Appl. Catal. A-Gen.* 382, 148–157. doi: 10.1016/j.apcata.2010.04.027
- Bobadilla, L. F., Santos, J. L., Ivanova, S., Odriozola, J. A., and Urakawa, A. (2018). Unravelling the role of oxygen vacancies in the mechanism of the reverse water-gas shift reaction by operando drifts and ultraviolet-visible spectroscopy. *ACS Catal.* 8, 7455–7467. doi: 10.1021/acscatal.8b02121
- Bogolowski, N., Batalla, B. S., Shin, B., and Drillet, J. F. (2020). Activity of  $\text{La}_{0.75}\text{Sr}_{0.25}\text{Cr}_{0.5}\text{Mn}_{0.5}\text{O}_{3-\delta}$ ,  $\text{Ni}_3\text{Sn}_2$  and Gd-doped  $\text{CeO}_2$  towards the reverse water-gas shift reaction and carburisation for a high temperature  $\text{H}_2\text{O}/\text{CO}_2$  co-electrolysis. *RSC Adv.* 10, 10285–10296. doi: 10.1039/D0RA00362j
- Brennfürher, A., Neuman, H., and Beller, M. (2009). Palladium-catalyzed carbonylation reactions of aryl halides and related compounds. *Angew. Chem. Int. Ed.* 48, 4114–4133. doi: 10.1002/anie.200900013
- Burri, D. R., Choi, K. M., Han, S. C., Burri, A., and Park, S. E. (2007). Selective conversion of ethylbenzene into styrene over  $\text{K}_2\text{O}/\text{TiO}_2$ -ZrO<sub>2</sub> catalysts: unified effects of  $\text{K}_2\text{O}$  and  $\text{CO}_2$ . *J. Mol. Catal. A-Chem.* 269, 58–63. doi: 10.1016/j.molcata.2006.12.021
- Cadi-Essadek, A., Roldan, A., Aparicio-Anglès, X., and de Leeuw, N. H. (2018).  $\text{CO}_2$  and  $\text{H}_2$  adsorption and reaction at  $\text{Ni}_n/\text{YSZ}(111)$  interfaces: a density functional theory study. *J. Phys. Chem. C* 122, 19463–19472. doi: 10.1021/acs.jpcc.8b03488
- Cao, Z., Guo, L., Liu, N. Y., Zheng, X. L., Li, W. L., Shi, Y. Y., et al. (2016). Theoretical study on the reaction mechanism of reverse water-gas shift reaction using a Rh–Mo<sub>6</sub>S<sub>8</sub> cluster. *RSC Adv.* 6, 108270–108279. doi: 10.1039/C6RA23855F
- Carrasquillo-Flores, R., Ro, L., Kumbhalkar, M. D., Burt, S., Carrero, C. A., Alba-Rubio, A. C., et al. (2015). Reverse water-gas shift on interfacial sites formed by deposition of oxidized molybdenum moieties onto gold nanoparticles. *J. Am. Chem. Soc.* 137, 10317–10325. doi: 10.1021/jacs.5b05945
- Centi, G., and Perathoner, S. (2009). Opportunities and prospects in the chemical recycling of carbon dioxide to fuels. *Catal. Today* 148, 191–205. doi: 10.1016/j.cattod.2009.07.075
- Chen, C. S., and Cheng, W. H. (2002). Study on the mechanism of CO formation in reverse water gas shift reaction over Cu/SiO<sub>2</sub> catalyst by pulse reaction, TPD and TPR. *Catal. Lett.* 83, 121–126. doi: 10.1023/A:1021006718974
- Chen, C. S., Cheng, W. H., and Lin, S. S. (2000). Mechanism of CO formation in reverse water-gas shift reaction over Cu/Al<sub>2</sub>O<sub>3</sub> catalyst. *Catal. Lett.* 68, 45–48. doi: 10.1023/A:1019071117449
- Chen, C. S., Cheng, W. H., and Lin, S. S. (2003). Study of reverse water gas shift reaction by TPD, TPR and CO<sub>2</sub> hydrogenation over potassium-promoted Cu/SiO<sub>2</sub> catalyst. *Appl. Catal. A-Gen.* 238, 55–67. doi: 10.1016/S0926-860X(02)00221-1
- Chen, C. S., Cheng, W. H., and Lin, S. S. (2004). Study of iron-promoted Cu/SiO<sub>2</sub> catalyst on high temperature reverse water gas shift reaction. *Appl. Catal. A Gen.* 257, 97–106. doi: 10.1016/S0926-860X(03)00637-9
- Chen, X. D., Su, X., Duan, H. M., Liang, B. L., Huang, Y. Q., and Zhang, T. (2017a). Catalytic performance of the Pt/TiO<sub>2</sub> catalysts in reverse water gas shift reaction: Controlled product selectivity and a mechanism study. *Catal. Today* 281, 312–318. doi: 10.1016/j.cattod.2016.03.020
- Chen, X. D., Su, X., Liang, B. L., Yang, X. L., Ren, X. Y., Duan, H. M., et al. (2016). Identification of relevant active sites and a mechanism study for reverse water gas shift reaction over Pt/CeO<sub>2</sub> catalysts. *J. Energy Chem.* 25, 1051–1057. doi: 10.1016/j.jechem.2016.11.011
- Chen, X. D., Su, X. H., Su, Y., Liu, X. Y., Miao, S., Zhao, Y. H., et al. (2017b). Theoretical insights and the corresponding construction of supported metal catalysts for highly selective CO<sub>2</sub> to CO conversion. *ACS Catal.* 7, 4613–4620. doi: 10.1021/acscatal.7b00903
- Chen, Y., Galinsky, N., Wang, Z., and Li, F. (2014). Investigation of perovskite supported composite oxide oxides for chemical looping conversion of syngas. *Fuel* 134, 521–530. doi: 10.1016/j.fuel.2014.06.017
- Choi, P. H., Jun, W. K., Lee, J. S., Choi, J. M., and Lee, W. K. (1996). Hydrogenation of carbon dioxide over alumina supported Fe-K catalysts. *Catal. Lett.* 40, 115–118. doi: 10.1007/BF00807467
- Connor, C. P., and Holland, P. L. (2017). Coordination chemistry insights into the role of alkali metal promoters in dinitrogen reduction. *Catal. Today* 286, 21–40. doi: 10.1016/j.cattod.2016.08.014
- Cosultchi, A., Pérez-Luna, M., Morales-Serna, J. A., and Salmón, M. (2012). Characterization of modified Fischer-Tropsch catalysts promoted with alkaline metals for higher alcohol synthesis. *Catal. Lett.* 142, 368–377. doi: 10.1007/s10562-012-0765-9
- Dai, B., Cao, S. Q., Xie, H. M., Zhou, G. L., and Chen, S. M. (2018). Reduction of CO<sub>2</sub> to CO via reverse water-gas shift reaction over CeO<sub>2</sub> catalyst. *Korean J. Chem. Eng.* 35, 421–427. doi: 10.1007/s11814-017-0267-y
- Daza, Y. A., Kent, R. A., Yung, M. M., and Kuhn, J. N. (2014). Carbon dioxide conversion by reverse water-gas shift chemical looping on perovskite-type oxides. *Int. Eng. Chem. Res.* 53, 5828–5837. doi: 10.1021/ie5002185
- Daza, Y. A., Maiti, D., Hare, B. J., Bhethanabotla, V. R., Kuhn, J. N., and More, C. U. (2016). More problems: decreased CO<sub>2</sub> conversion ability by Cu-doped  $\text{La}_{0.75}\text{Sr}_{0.25}\text{FeO}_3$  perovskite oxides. *Surf. Sci.* 648, 92–99. doi: 10.1016/j.susc.2015.11.017
- Daza, Y. A., Maiti, D., Kent, R. A., Bhethanabotla, V. R., and Kuhn, J. N. (2015). Isothermal reverse water gas shift chemical looping on  $\text{La}_{0.75}\text{Sr}_{0.25}\text{Co}_{1-\gamma}\text{Fe}_\gamma\text{O}_3$  perovskite-type oxides. *Catal. Today* 258, 691–698. doi: 10.1016/j.cattod.2014.12.037
- de Lima, R. K. C., Batista, M. S., Wallau, M., Sanches, E. A., Mascarenhas, Y. P., and Urquieta-González, E. A. (2009). High specific surface area LaFeCo perovskite synthesis by nanocasting and catalytic behavior in the reduction of NO with CO. *Appl. Catal. B-Environ.* 9, 441–450. doi: 10.1016/j.apcatb.2009.04.004
- Delgado, J. J., José, M. C., López-Haro, M., del R. E., Calvino, J. J., Serafin, B., et al. (2011). Recent progress in chemical characterization of supported gold catalysts: CO adsorption on Au/ceira-zirconia. *Chem. Lett.* 40, 1210–1216. doi: 10.1246/cl.2011.1210
- Diebold, U. (2003). The surface science of titanium dioxide. *Sur. Sci. Rep.* 48, 53–229. doi: 10.1016/S0167-5729(02)00100-0
- Dong, Q., Yin, S., Guo, C. S., and Sato, T. (2012). Ce<sub>0.5</sub>Zr<sub>0.4</sub>Sn<sub>0.1</sub>O<sub>2</sub>/Al<sub>2</sub>O<sub>3</sub> catalysts with enhanced oxygen storage capacity and high CO oxidation activity. *Catal. Sci. Technol.* 2, 2521–2524. doi: 10.1039/c2cy20425h
- Feyzi, M., Irandoust, M., and Mirzaei, A. A. (2011). Effects of promoters and calcination conditions on the catalytic performance of iron-manganese catalysts for fisher-tropsch synthesis. *Fuel Process. Technol.* 92, 1136–1143. doi: 10.1016/j.fuproc.2011.01.010
- Fornero, E. L., Chiavassa, D. L., Bonivardi, A. L., and Baltanás, M. A. (2017). Transient analysis of the reverse water gas shift reaction on Cu/ZrO<sub>2</sub> and Ga<sub>2</sub>O<sub>3</sub>/Cu/ZrO<sub>2</sub> catalysts. *J. CO<sub>2</sub> Util.* 22, 289–298. doi: 10.1016/j.jcou.2017.06.002
- Fu, Q., and Wagner, T. (2007). Interaction of nanostructured metal overlayers with oxide surfaces. *Sur. Sci. Rep.* 62, 431–498. doi: 10.1016/j.surfrep.2007.07.001
- Fujita, S. L., Usui, M., and Takezawa, N. (1992). Mechanism of the reverse water gas shift reaction over Cu/ZnO catalyst. *J. Catal.* 134, 220–225. doi: 10.1016/0021-9517(92)90223-5
- Gálvez, M. E., Ascaso, S., and Moliner, R., Lázaro MJ (2013). Influence of the alkali promoter on the activity and stability of transition metal (Cu, Co, Fe) based structured catalysts for the simultaneous removal of soot and NO<sub>x</sub>. *Top Catal.* 56, 493–498. doi: 10.1007/s11244-013-0004-7
- Gao, S., Lin, Y., Jiao, X. C., Sun, Y. F., Luo, Q. Q., Zhang, W. H., et al. (2016). Partially oxidized atomic cobalt layers for carbon dioxide electroreduction to liquid fuel. *Nature* 529, 68–71. doi: 10.1038/nature16455
- Garin, F. (2001). Mechanism of NO<sub>x</sub> decomposition. *Appl. Catal. A-Gen.* 222, 183–219. doi: 10.1016/S0926-860X(01)00827-4
- Ghoussoub, M., Yadav, S., Ghuman, K. K., Ozin, G. A., and Singh, C. V. (2016). Metadynamics-biased ab initio molecular dynamics study of heterogeneous CO<sub>2</sub> reduction via surface frustrated lewis pairs. *ACS Catal.* 6, 7109–7117. doi: 10.1021/acscatal.6b01545
- Ghuman, K. K., Wood, T. E., Hoch, L. B., Mims, C. A., Ozin, G. A., and Singh, C. V. (2015). Illuminating CO<sub>2</sub> reduction on frustrated lewis pair surfaces: investigating the role of surface hydroxides and oxygen vacancies on nanocrystalline In<sub>2</sub>O<sub>3-x</sub>(OH)<sub>y</sub>. *Phys. Chem. Chem. Phys.* 17, 14623–14635. doi: 10.1039/C5CP02613J
- Gines, M. J. L., March, A. J., and Apesteguía, C. R. (1997). Kinetic study of the reverse water-gas shift reaction over CuO/ZnO/Al<sub>2</sub>O<sub>3</sub> catalysts. *Appl. Catal. A-Gen.* 154, 155–171. doi: 10.1016/S0926-860X(96)00369-9

- Goguet, A., Meunier, F., Breen, J. P., Burch, R., Petch, M. I., and Ghenciu, A. F. (2004b). Study of the origin of the deactivation of a Pt/CeO<sub>2</sub> catalyst during reverse water gas shift (RWGSR) reaction. *J. Catal.* 226, 382–392. doi: 10.1016/j.jcat.2004.06.011
- Goguet, A., Meunier, F. C., Tibiletti, D., Breen, J. P., and Burch, T. (2004a). Spectrokinetic investigation of reverse water-gas-shift reaction intermediates over a Pt/CeO<sub>2</sub> catalyst. *J. Phys. Chem. B* 108, 20240–20246. doi: 10.1021/jp047242w
- Goguet, A., Shekhtman, S. O., Burch, R., Hardacre, C., Meunier, F. C., and Yablonsky, G. S. (2016). Pulse-response TAP studies of the reverse water-gas shift reaction over a Pt/CeO<sub>2</sub> catalyst. *J. Catal.* 237, 102–110. doi: 10.1016/j.jcat.2005.10.020
- Graciani, J., Mudiyansele, K., Xu, F., Baber, A. E., Evans, J., Senanayake, S. D., et al. (2014). Highly active copper-ceria and copper-ceria-titania catalysts for methanol synthesis from CO<sub>2</sub>. *Science* 345, 546–550. doi: 10.1126/science.1253057
- Han, Y. Q., Xu, H. T., Su, Y. Q., Xu, Z. L., Wang, K. F., and Wang, W. Z. (2019). Noble metal (Pt, Au@Pd) nanoparticles supported on metal organic framework (MOF-74) nanoshuttles as high-selectivity CO<sub>2</sub> conversion catalysts. *J. Catal.* 370, 70–78. doi: 10.1016/j.jcat.2018.12.005
- Hare, B. J., Maiti, D., Daza, Y. A., Bhethanabotla, V. R., and Kuhn, J. N. (2018). Enhanced CO<sub>2</sub> conversion to CO by silica-supported perovskite oxide at low temperatures. *ACS Catal.* 8, 3021–3029. doi: 10.1021/acscatal.7b03941
- Hare, B. J., Maiti, D., Ramani, S., Ramos, A. E., and Bhethanabotla, V. R. (2019). Thermochemical conversion of carbon dioxide by reverse water-gas shift chemical looping using supported perovskite oxides. *Catal. Today* 323, 225–232. doi: 10.1016/j.cattod.2018.06.002
- He, Y. L., Yang, K. R., Yu, Z. W., Fishman, Z. S., Achola, L. A., and Tobin, Z. M. (2019). Catalytic manganese oxide nanostructures for the reverse water gas shift reaction. *Nanoscale* 11, 16677–16688. doi: 10.1039/C9NR06078B
- Huš M., Dasireddy, V. D. B. C., Stefancic, N. S., and Likozar, B. (2017). Mechanism, kinetics and thermodynamics of carbon dioxide hydrogenation to methanol on Cu/ZnAl<sub>2</sub>O<sub>4</sub> spinel-type heterogeneous catalysts. *Appl. Catal. B-Environ.* 207, 267–278. doi: 10.1016/j.apcatb.2017.01.077
- Ishito, N., Hara, K. J., Nakajima, K., and Fukuoka, A. (2016). Selective synthesis of carbon monoxide via formates in reverse water-gas shift reaction over alumina-supported gold catalyst. *J. Energy Chem.* 25, 306–310. doi: 10.1016/j.jechem.2015.12.005
- Jafari, A., Ebadi, A., and Sahedbedifar, S. (2019). Effect of iron oxide precursor on the properties and ammonia synthesis activity of fused iron catalysts. *React. Kinet. Mech. Cat.* 126, 307–325. doi: 10.1007/s11144-018-1498-6
- Jing, H. J., Li, Q. H., Wu, J., Liu, D. W., and Wu, K. C. (2019). Theoretical study of the reverse water gas shift reaction on copper modified β-Mo<sub>2</sub>C (001) surfaces. *J. Phys. Chem. C* 123, 1235–1251. doi: 10.1021/acs.jpcc.8b09884
- Jones, J. H. (2000). Te cativa process for the manufacture of acetic acid. Iridium catalyst improves productivity in an established industrial process. *Platin. Met. Rev.* 44, 94–105.
- Joo, O. S., and Jung, K. D. (2003). Stability of ZnAl<sub>2</sub>O<sub>4</sub> catalyst for reverse-water-gas-shift reaction (RWGSR). *B Korean Chem. Soc.* 24:1. doi: 10.5012/bkcs.2003.24.1.086
- Kae, H. K., Park, J. L., Park, E. J., Dim, Y. D., and SUhm, H. (2014). Dopant effect of barium zirconate-based perovskite-type catalysts for the intermediate-temperature reverse water gas shift reaction. *ACS Catal.* 4, 3117–3122. doi: 10.1021/cs500476e
- Kang, J., Czaja, A. D., and Gulians, V. V. (2017). Carbon dioxide as feedstock in selective oxidation of propane. *Eur. J. Inorg. Chem.* 2017, 4757–4762. doi: 10.1002/ejic.201701049
- Karelovic, A., Galdames, G., Median, J. C., Yévenes, C., Barra, Y., and Jiménez, R. (2019). Mechanism and structure sensitivity of methanol synthesis from CO<sub>2</sub> over SiO<sub>2</sub>-supported Cu nanoparticles. *J. Catal.* 369, 419–426. doi: 10.1016/j.jcat.2018.11.012
- Katta, L., Sudarsamam, P., Thirumurthulu, G., and Reddy, B. M. (2010). Doped nanosized ceria solid solutions for low temperature soot oxidation: zirconium versus lanthanum promoters. *Appl. Catal. B-Environ.* 101, 101–108. doi: 10.1016/j.apcatb.2010.09.012
- Kattel, S., Liu, P., and Chen, J. G. (2017). Tuning selectivity of RWGSR reactions at the metal/oxide interface. *J. Am. Chem. Soc.* 139, 9739–9754. doi: 10.1021/jacs.7b05362
- Kattel, S., Yan, B. H., Chen, J. G. G., and Liu, P. (2016a). RWGSR on Pt, Pt/SiO<sub>2</sub> and Pt/TiO<sub>2</sub>: importance of synergy between Pt and oxide support. *J. Catal.* 343, 115–126. doi: 10.1016/j.jcat.2015.12.019
- Kattel, S., Yu, W. T., Yang, X. F., Yan, B. H., Huang, Y. Q., Wan, W. M., et al. (2016b). CO<sub>2</sub> hydrogenation over oxide-supported PtCo catalysts the role of the oxide support in determining the product selectivity. *Angew. Chem. Int. Ed.* 55, 7968–7973. doi: 10.1002/anie.201601661
- Kharaji, A. G., Shariati, A., and Ostadi, M. (2014). Development of Ni-Mo/Al<sub>2</sub>O<sub>3</sub> catalyst for reverse water gas shift (RWGSR) reaction. *J. Nanosci. Nanotechnol.* 14, 6841–6847. doi: 10.1166/jnn.2014.8962
- Kharaji, A. G., Shariati, A., and Takassi, M. A. (2013). A novel γ-alumina supported Fe-Mo bimetallic catalyst for reverse water gas shift reaction. *Chinese J. Chem. Eng.* 21, 1007–1014. doi: 10.1016/S1004-9541(13)60573-X
- Kim, D. H., Han, S. W., Yoon, H. S., and Kim, Y. D. (2015). Reverse water gas shift reaction catalyzed by Fe nanoparticles with high catalytic activity and stability. *J. Ind. Eng. Chem.* 23, 67–71. doi: 10.1016/j.jiec.2014.07.043
- Kim, S. S., Lee, H. H., and Hong, S. C. (2012a). The effect of the morphological characteristics of TiO<sub>2</sub> supports on the reverse water-gas shift reaction over Pt/TiO<sub>2</sub> catalysts. *Appl. Catal. B-Environ.* 119–120, 100–108. doi: 10.1016/j.apcatb.2012.02.023
- Kim, S. S., Lee, H. H., and Hong, S. C. (2012b). A study on the effect of support's reducibility on the reverse water-gas shift reaction over Pt catalysts. *Appl. Catal. A-Gen.* 423–424, 100–107. doi: 10.1016/j.apcata.2012.02.021
- Kim, S. S., Park, K. H., and Hong, S. C. (2013). A study of the selectivity of the reverse water-gas-shift reaction over Pt/TiO<sub>2</sub> catalysts. *Fuel Process. Technol.* 108, 47–54. doi: 10.1016/j.fuproc.2012.04.003
- Klankermayer, J., Wesselbaum, S., Beydoun, K., and Leitner, W. (2016). Selective catalytic synthesis using the combination of carbon dioxide and hydrogen: catalytic chess at the interface of energy and chemistry. *Angew. Chem. Int. Ed.* 55, 7296–7343. doi: 10.1002/anie.201507458
- Klvana, D., Kirchnerová J., and Tofan, C. (1999). Catalytic decomposition of nitric oxide by perovskites. *Korean J. Chem. Eng.* 16, 470–477. doi: 10.1007/BF02698270
- Kovacevic, M., Mojet, B. L., van Ommen, J. G., and Lefferts, L. (2016). Effects of morphology of cerium oxide catalysts for reverse water gas shift reaction. *Catal. Lett.* 146, 770–777. doi: 10.1007/s10562-016-1697-6
- Krstajić, V. N., Lačnjevac, C. M., Jakšić J. M., and Jakšić M. M. (2008). Interactive supported electrocatalysts and spillover effect in electrocatalysis for hydrogen and oxygen electrode reactions. *Chem. Ind. Chem. Q.* 14, 119–136. doi: 10.2298/CICEQ0802119J
- Kwak, J. H., Kovarik, L., and Szanyi, J. (2013a). Heterogeneous catalysis on atomically dispersed supported metals: CO<sub>2</sub> reduction on multifunctional Pd catalysts. *ACS Catal.* 3, 2094–2100. doi: 10.1021/cs4001392
- Kwak, J. H., Kovarik, L., and Szanyi, J. (2013b). CO<sub>2</sub> reduction on supported Ru/Al<sub>2</sub>O<sub>3</sub> catalysts: cluster size dependence of product selectivity. *ACS Catal.* 3, 2449–2455. doi: 10.1021/cs400381f
- Li, D., Ichikuni, N., Shimazu, S., and Uematsu, T. (1998). Catalytic properties of sprayed Ru/Al<sub>2</sub>O<sub>3</sub> and promoter effects of alkali metals in RWGSR. *Appl. Catal. A-Gen.* 172, 351–358. doi: 10.1016/S0926-860X(98)00139-2
- Li, F., Luo, S., Sun, Z., Bao, X., and Fan, L. (2011). Role of metal oxide support in redox reactions of iron oxide for chemical looping applications; experiments and density functional theory calculations. *Energy Environ. Sci.* 4, 3661–3667. doi: 10.1039/c1ee01325d
- Li, L., Hu, L. P., Li, J., and Wei, Z. D. (2015). Enhanced stability of Pt nanoparticle electrocatalysts for fuel cells. *Nano Res.* 8, 418–440. doi: 10.1007/s12274-014-0695-5
- Li, R. X., Yabe, S., Yamashita, M., Momose, S., Yoshida, S., Yin, S., et al. (2002). UV-shielding properties of zinc oxide-doped ceria fine powders derived via soft solution chemical routes. *Mater. Chem. Phys.* 75, 39–44. doi: 10.1016/S0254-0584(02)00027-5
- Li, S. W., Xu, Y., Chen, Y. F., Li, W. Z., Lin, L. L., Li, M. Z., et al. (2017). Tuning the selectivity of catalytic carbon dioxide hydrogenation over iridium/cerium oxide catalysts with a strong metal-support interaction. *Angew. Chem. Int. Ed.* 56, 10761–10765. doi: 10.1002/anie.201705002
- Liang, B., Duan, H. M., Su, X., Chen, X. D., Huang, Y. Q., Chen, X. W., et al. (2017). Promoting role of potassium in the reverse water gas shift reaction on Pt/mullite catalyst. *Catal. Today* 281, 319–326. doi: 10.1016/j.cattod.2016.02.051

- Lin, B., Liu, Y., Heng, L., Ni, J., Lin, J. X., and Jiang, L. L. (2018a). Effect of barium and potassium promoter on Co/CeO<sub>2</sub> catalysts in ammonia synthesis. *J. Rare Earth*. 36, 703–707. doi: 10.1016/j.jre.2018.01.017
- Lin, F. J., Delmelle, R., Vinodkumar, T., Reddy, B. M., Wokaun, A., and Alkneit, I. (2015). Correlation between the structural characteristics, oxygen storage capacities and catalytic activities of dual-phase Zn-modified ceria nanocrystals. *Catal. Sci. Technol.* 5, 3556–3567. doi: 10.1039/C5CY00351B
- Lin, L. L., Yao, S. Y., Liu, Z. Y., Zhang, F., Li, N., Vovchok, D., et al. (2018b). *In situ* characterization of Cu/CeO<sub>2</sub> nanocatalysts for RWGSR: morphological effects of nanostructured ceria on the catalytic activity. *J. Phys. Chem. C* 122, 12934–12943. doi: 10.1021/acs.jpcc.8b03596
- Lin, W., Stocker, K. M., and Schatz, G. C. (2017). Mechanisms of hydrogen-assisted CO<sub>2</sub> reduction on nickel. *J. Am. Chem. Soc.* 139, 4663–4666. doi: 10.1021/jacs.7b01538
- Liu, B. W., Ju, Y. W., Abe, T., and Kawamoto, K. (2015). Dispersion and distribution of bimetallic oxides in SBA-15, and their enhanced activity for reverse water gas shift reaction. *Iron. Chem. Front.* 2, 741–748. doi: 10.1039/C5QI00062A
- Liu, D. Y., Li, Y. Y., Kottwitz, M., Yan, B. H., Yao, S. Y., Gamalski, A., et al. (2018). Identifying dynamic structural changes of active sites in Pt-Ni bimetallic catalysts using multimodal approaches. *ACS Catal.* 5, 4120–4131. doi: 10.1021/acscatal.8b00706
- Liu, L., Das, S. L., Chen, T. J., Dewangan, N., Ashok, J., Xi, S. B., et al. (2020). Low temperature catalytic reverse water-gas shift reaction over perovskite catalysts in DBD plasma. *Appl. Catal. B-Environ.* 265:118573. doi: 10.1016/j.apcatb.2019.118573
- Liu, L. N., Fan, F., Bai, M. M., Xue, F., Ma, X. R., Jiang, Z., et al. (2019). Mechanistic study of methanol synthesis from CO<sub>2</sub> hydrogenation on Rh-doped Cu(111) surfaces. *Mol. Catal.* 466, 26–36. doi: 10.1016/j.mcat.2019.01.009
- Liu, X. Y., Wang, A. Q., Zhang, T., and Mou, C. Y. (2013). Catalysis by gold: new insights into the support effect. *Nano Today* 8, 403–416. doi: 10.1016/j.nantod.2013.07.005
- Liu, Y., and Liu, D. Z. (1999). Study of bimetallic Cu-Ni/ $\gamma$ -Al<sub>2</sub>O<sub>3</sub> catalysts for carbon dioxide hydrogenation. *Int. J. Hydrogen. Energy* 24, 351–354. doi: 10.1016/S0360-3199(98)00038-X
- Liu, Y., Zhang, C. H., Wang, Y., Li, Y., Hao, X., Bai, L., et al. (2008). Effect of co-feeding carbon dioxide on Fischer-Tropsch synthesis over an iron-manganese catalyst in a spinning basket reactor. *Fuel Process. Technol.* 89, 234–241. doi: 10.1016/j.fuproc.2007.11.002
- Lu, B. W., and Kawamoto, K. (2014). Preparation of mesoporous CeO<sub>2</sub> and monodispersed NiO particles in CeO<sub>2</sub>, and enhanced selectivity of NiO/CeO<sub>2</sub> for reverse water gas shift reaction. *Mater. Res. Bull.* 53, 70–78. doi: 10.1016/j.materresbull.2014.01.043
- Maiti, D., Daza, Y. A., Yung, M. M., Kuhn, J. N., and Bhethanabotla, V. R. (2016). Oxygen vacancy formation characteristics in the bulk and across different surface terminations of La<sub>(1-x)</sub>Fe<sub>(1-y)</sub>Co<sub>y</sub>O<sub>(3-δ)</sub> perovskite oxides for CO<sub>2</sub> conversion. *J. Mater. Chem. A* 4, 5137–5148. doi: 10.1039/C5TA10284G
- Maitlis, P. M., Haynes Maitlis, A., Sunley, G. J., and Howard, M. J. (1996). Methanol carbonylation revisited: thirty years on. *J. Chem. Soc. Dalton.* 112, 2187–2196. doi: 10.1039/dt9960002187
- Masui, T., Fujiwara, K., Machida, K., and Adachi, G. (1997). Characterization of Cerium(IV) oxide ultrafine particles prepared using reversed micelles. *Chem. Mater.* 9, 2197–2204. doi: 10.1021/cm970359v
- Matsubu, J. C., Yang, V. N., and Christopher, P. (2015). Isolated metal active site concentration and stability control catalytic CO<sub>2</sub> reduction selectivity. *J. Am. Chem. Soc.* 137, 3076–3084. doi: 10.1021/ja5128133
- Matsubu, J. C., Zhang, Y., DeRita, L., Marinkovic, N. S., Chen, J. G., Graham, G. W., et al. (2017). Adsorbate-mediated strong metal-support interactions in oxide-supported Rh catalysts. *Nat. Chem.* 9, 120–127. doi: 10.1038/nchem.2607
- Mikkelsen, M., Jørgensen, M., and Krebs, F. C. (2010). The teraton challenge. A review of fixation and transformation of carbon dioxide. *Energy Environ. Sci.* 3, 43–81. doi: 10.1039/B912904A
- Millet, M. M., Algara-Siller, G., Wrabetz, S., Mazheika, A., Girgsdies, F., and Teschner, D. (2019). Ni single atom catalysts for CO<sub>2</sub> activation. *J. Chem. Soc.* 141, 2451–2461. doi: 10.1021/jacs.8b11729
- Min, B. K., Santra, A. K., and Goodman, D. W. (2003). Understanding silicasupported metal catalysts: Pd/silica as a case study. *Catal. Today* 85, 113–124. doi: 10.1016/S0920-5861(03)00380-8
- Mirzaei, A. A., R., Habibpour Faizi, M., and Kashi, E. (2006). Characterization of iron-cobalt oxide catalysts: effect of different supports and promoters upon the structure and morphology of precursors and catalysts. *Appl. Catal. A-Gen.* 301, 272–283. doi: 10.1016/j.apcata.2005.12.022
- Morse, J. R., Juneau, M., Baldwin, J. W., Porosoff, M. D., and Willauer, H. D. (2020). Alkali promoted tungsten carbide as a selective catalysts for the reverse water gas shift reaction. *J. CO<sub>2</sub> Util.* 35, 38–46. doi: 10.1016/j.jcou.2019.08.024
- Mukherjee, D., Park, S. E., and Reddy, B. M. (2016). CO<sub>2</sub> as a soft oxidant for oxidative dehydrogenation reaction: an eco-benign process for industry. *J. CO<sub>2</sub> Util.* 16, 301–312. doi: 10.1016/j.jcou.2016.08.005
- Naito, S., Aida, S. G., Kasahara, T., and Miyao, T. H. (2006). Infrared spectroscopic study on the reaction mechanism of CO hydrogenation over Pd/CeO<sub>2</sub>. *Res. Chem. Intermediat.* 32, 279–290. doi: 10.1163/15685670677346444
- Nakamura, I., Fujitani, T., Uchijima, T., and Nakamura, J. (1998). The synthesis of methanol and the reverse water-gas shift reaction over Zn-deposited Cu(100) and Cu(110) surfaces: comparison with Zn/Cu(111). *Surf. Sci.* 400, 387–400. doi: 10.1016/S0039-6028(97)00899-6
- Neophytides, S. G., Zafeiratos, S., Papakonstantinou, G. D., Jaksic, J. M., Paloukis, F. E., and Jaksic, M. M. (2005). Extended brewer hypohyper-d-interionic bonding theory II. strong metal-support interaction grafting of composite electrocatalysts. *Int. J. Hydrog. Energy* 30, 393–410. doi: 10.1016/j.ijhydene.2004.07.005
- Nielsen, D. U., Hu, X. M., Daasbjerg, K., and Skrydstrup, T. (2018). Chemically and electrochemically catalysed conversion of CO<sub>2</sub> to CO with follow-up utilization to value-added chemicals. *Nat. Catal.* 1, 244–254. doi: 10.1038/s41929-018-0051-3
- Nitarori, T., Ichiki, T., and Misono, M. (1988). Catalytic properties of perovskite-type mixed oxides (ABO<sub>3</sub>) consisting of rare earth and 3d transition metals. The roles of the A- and B-site ions. *B. Chem. Soc. Jpn* 61, 621–626. doi: 10.1246/bcsj.61.621
- Obalová, L., Karásková, K., Wach, A., Kustrowski, P., Mamulová-Kutláková K., Michalik, S., et al. (2013). Alkali metals as promoters in Co-Mn-Al mixed oxide for N<sub>2</sub>O decomposition. *Appl. Catal. A-Gen.* 462–463, 227–235. doi: 10.1016/j.apcata.2013.05.011
- Okabe, K., Takahara, I., Inaba, M., Murata, K., and Yoshimura, Y. (2007). Effects of Ru precursors on activity of Ru-SiO<sub>2</sub> catalysts prepared by alkoxide method in Fisher-Tropsch synthesis. *J. Jpn. Petrol. Inst.* 50, 65–68. doi: 10.1627/jpi.50.65
- Okemoto, A., Harada, M. R., Ishizaka, T., Hiyoshi, N., and Sato, K. (2020). Catalytic performance of Mo<sub>3</sub>/FAU zeolite catalysts modified by Cu for reverse water gas shift reaction. *Appl. Catal. A-Gen.* 592:117415. doi: 10.1016/j.apcata.2020.117415
- Pacultová, K., Drašíková V., Chromčáková Ž., Bílková T., Kutláková, K. M., Kotarba, A., et al. (2017). On the stability of alkali metal promoters in Co mixed oxides during direct NO catalytic decomposition. *J. Mol. Catal. A Chem.* 428, 33–40. doi: 10.1016/j.molcata.2016.11.038
- Panaritis, C., Zgheib, J., Ebrahim, S. A. H., Couillard, M., and Baranova, E. A. (2020). Electrochemical in-situ activation of Fe-oxide nanowires for the reverse water gas shift reaction. *Appl. Catal. B-Environ.* 269:118826. doi: 10.1016/j.apcatb.2020.118826
- Panaritis, C., Edake, M., Couillard, M., Einakchi, R., and Baranova, E. A. (2018). Insight towards the role of ceria-based supports for reverse water gas shift reaction over RuFe nanoparticles. *J. CO<sub>2</sub> Util.* 26, 350–358. doi: 10.1016/j.jcou.2018.05.024
- Park, S. W., Joo, O. S., Jung, K. D., Kim, H., and Han, S. H. (2000). ZnO/Cr<sub>2</sub>O<sub>3</sub> catalyst for reverse-water-gas shift reaction of CAMERE process. *Korean J. Chem. Eng.* 17, 719–722. doi: 10.1007/BF02699123
- Park, S. W., Joo, O. S., Jung, K. D., Kim, H., and Han, S. H. (2001). Development of ZnO/Al<sub>2</sub>O<sub>3</sub> catalyst for reverse-water-gas-shift reaction of CAMERE (carbon dioxide hydrogenation to form methanol via a reverse-water-gas-shift reaction) process. *Appl. Catal. A-Gen.* 211, 81–90. doi: 10.1016/S0926-860X(00)00840-1
- Pastor-Pérez, L., Shah, M., Saché L. E., and Reina, T. R. (2018). Improving Fe/Al<sub>2</sub>O<sub>3</sub> catalysts for the reverse water-gas shift reaction: on the effect of Cs as activity/selectivity promoter. *Catalysts* 8:608. doi: 10.3390/catal8120608
- Peña, M. A., and Fierro, J. L. G. (2001). Chemical structures and performance of perovskite oxides. *Chem. Rev.* 101, 1981–2017. doi: 10.1021/cr980129f
- Porosoff, M. D., and Chen, J. G. (2013). Trends in the catalytic reduction of CO<sub>2</sub> by hydrogen over supported monometallic and bimetallic catalysts. *J. Catal.* 301, 30–37. doi: 10.1016/j.jcat.2013.01.022

- Porosoff, M. D., Yan, B. H., and Chen, J. G. (2016). Catalytic reduction of CO<sub>2</sub> by H<sub>2</sub> for synthesis of CO, methanol and hydrocarbons: challenges and opportunities. *Energ. Environ. Sci.* 9: 62–73. doi: 10.1039/C5EE02657A
- Porosoff, M. D., Yang, X. F., Boscoboinik, J. A., and Chen, J. G. (2014). Molybdenum carbide as alternative catalysts to precious metals for highly selective reduction of CO<sub>2</sub> to CO. *Angew. Chem. Int. Ed.* 53, 6705–6709. doi: 10.1002/anie.201404109
- Qian, C. X., Sun, W., Hung, D. L. H., Qiu, C. Y., Makaremi, M., Kumar, S. G. H., et al. (2019). Catalytic CO<sub>2</sub> reduction by palladium-decorated silicon-hydride nanosheets. *Nat. Catal.* 2, 46–54. doi: 10.1038/s41929-018-0199-x
- Radovic, M., Speakman, S. A., Allard, L. F., Payzant, E. A., Lara-Curzio, E., Kriven, W. M., et al. (2008). Thermal, mechanical and phase stability of LaCoO<sub>3</sub> in reducing and oxidizing environments. *J. Power Sour.* 184, 77–83. doi: 10.1016/j.jpowsour.2008.05.063
- Ranjabar, A., Irankhah, A., and Aghamiri, S. F. (2019). Catalytic activity of rare earth and alkali metal promoted (Ce, La, Mg, K) Ni/Al<sub>2</sub>O<sub>3</sub> nanocatalysts in reverse water gas shift reaction. *Res. Chem. Intermediat.* 45, 5125–5141. doi: 10.1007/s11164-019-03905-1
- Rao, K. N., Reddy, B. M., Abhishek, B., Seo, Y. H., Jiang, N. Z., and Park, S. E. (2009). Effect of ceria on the structure and catalytic activity of V<sub>2</sub>O<sub>5</sub>/TiO<sub>2</sub>-ZrO<sub>2</sub> for oxidehydrogenation of ethylbenzene to styrene utilizing CO<sub>2</sub> as soft oxidant. *Appl. Catal. B-Environ.* 91, 649–656. doi: 10.1016/j.apcatb.2009.07.003
- Reddy, B. M., Han, D. S., Jiang, N. Z., and Park, S. E. (2008). Dehydrogenation of ethylbenzene to styrene with carbon dioxide over ZrO<sub>2</sub>-based composite oxide catalysts. *Catal. Surv. Asia* 12, 56–69. doi: 10.1007/s10563-007-9039-8
- Reddy, B. M., Katta, L., and Thrimurthulu, G. (2010). Novel nanocrystalline Ce<sub>1-x</sub>La<sub>x</sub>O<sub>2-δ</sub> (x = 0.2) solid solutions: structural characteristics and catalytic performance. *Chem. Mater.* 22, 467–475. doi: 10.1021/cm903282w
- Riedel, T., Claeys, M., Schulz, H., Schaub, G., Nam, S. S., Jun, K. W., et al. (1999). Comparative study of fischer-tropsch synthesis with H<sub>2</sub>/CO and H<sub>2</sub>/CO<sub>2</sub> syngas using Fe- and Co-based catalysts. *Appl. Catal. A-Gen.* 186, 201–203. doi: 10.1016/S0926-860X(99)00173-8
- Ringuède A., and Fouletier, J. (2001). Oxygen reaction on strontium-doped lanthanum cobaltite dense electrodes at intermediate temperatures. *Solid State Ionics* 139, 167–177. doi: 10.1016/S0167-2738(01)00692-0
- Ro, I., Sener, C., Stadelman, T. M., Ball, M. R., Venegas, J. M., Burt, S. P., et al. (2016). Measurement of intrinsic catalytic activity of Pt monometallic and Pt-MoOx interfacial sites over visible light enhanced PtMoOx/SiO<sub>2</sub> catalyst in reverse water gas shift reaction. *J. Catal.* 344, 784–794. doi: 10.1016/j.jcat.2016.08.011
- Rogowski, J. (2019). TOF-SIMS study of morphology and chemical composition of wustite-based precursor and iron catalyst for ammonia synthesis. *Appl. Sur. Sci.* 469, 82–89. doi: 10.1016/j.apsusc.2018.10.271
- Roiaz, M., Monachino, E., Dri, C., Greiner, M., Knop-Gericke, A., Schlögl, R., et al. (2016). Reverse water-gas shift or Sabatier methanation on Ni(110)? Stable surface species at near ambient pressure. *J. Am. Chem. Soc.* 138, 4146–4154. doi: 10.1021/jacs.5b13366
- Ronda-Lloret, M., Rico-Francés, S., Sepúlveda-Escribano, A., and Ramos-Fernandez, E. V. (2018). CuOx/CeO<sub>2</sub> catalyst derived from metal organic framework for reverse water-gas shift reaction. *Appl. Catal. A-Gen.* 562, 28–36. doi: 10.1016/j.apcata.2018.05.024
- Royer, S., Duprez, D., and Kaliaguine, S. (2005). Role of bulk and grainboundary oxygen mobility in the catalytic oxidation activity of LaCo<sub>1-x</sub>Fe<sub>x</sub>O<sub>3</sub>. *J. Catal.* 234, 364–375. doi: 10.1016/j.jcat.2004.11.041
- Sache, E. L., Pastor-Pérez, L., Haycock, B. J., Villora-Picó J. J., Sepúlveda-Escribano, A., and Ramirez Reina, T. (2020). Switchable catalysts for chemical CO<sub>2</sub> recycling: A step forward in the methanation and reverse water-gas shift reactions. *ACS Sustain. Chem. Eng.* 11, 4614–4622. doi: 10.1021/acssuschemeng.0c00551
- Saeidi, S., Najari, S., Fazlollahi, F., Nikoo, M. F., Sefidkon, F., Klemes, J. J., et al. (2017). Mechanisms and kinetics of CO<sub>2</sub> hydrogenation to value-added products: A detailed review on current status and future trends. *Renew. Sust. Energ. Rev.* 80, 1292–1311. doi: 10.1016/j.rser.2017.05.204
- Sahbedelfar, S., and Takht Ravanchi, M. (2015). Carbon dioxide utilization for methane production: A thermodynamic analysis. *J. Petrol. Sci. Eng.* 134 14–22. doi: 10.1016/j.petrol.2015.07.015
- Schmale, K., Daniels, M., Buchheit, A., Grünebaum, M., Haase, L., Koops, S., et al. (2013). Influence of zinc oxide on the conductivity of ceria. *J. Electrochem. Soc.* 160, 1081–1087. doi: 10.1149/2.119309jes
- Shimoda, N., Kimura, Y., Kobayashi, Y., Kubota, J., and Satokawa, S. (2017). Ammonia synthesis over yttrium-doped barium zirconate and cerate-based perovskite-type oxide supported ruthenium catalysts. *Int. J. Hydrog. Energ.* 42, 29745–29755. doi: 10.1016/j.ijhydene.2017.10.108
- Silva-Calpa, L. D. R., Zonetti, P. C., Rodrigues, C. P., Alves, O. C., Appel, L. G., and de Aveliz, R. R. (2016). The Zn<sub>x</sub>Zr<sub>1-x</sub>O<sub>2-y</sub> solid solution on m-ZrO<sub>2</sub>: creating O vacancies and improving the m-ZrO<sub>2</sub> redox properties. *J. Mol. Catal. A-Chem.* 425, 166–173. doi: 10.1016/j.molcata.2016.10.008
- Su, X., Yang, X. F., Huang, Y. Q., Liu, B., and Zhang, T. (2019). Single-atom catalysis toward efficient CO<sub>2</sub> conversion to CO and formate products. *Acc. Chem. Res.* 52, 656–664. doi: 10.1021/acs.accounts.8b00478
- Su, X., Yang, X. L., Zhao, B., and Huang, Y. Q. (2017). Designing of highly selective and high-temperature enduring RWGSR heterogeneous catalysts: recent advances and the future directions. *J. Energy Chem.* 26, 854–867. doi: 10.1016/j.jechem.2017.07.006
- Sun, C. W., Li, H., and Chen, L. Q. (2012). Nanostructured ceria-based materials: synthesis, properties, and applications. *Energy Environ. Sci.* 5, 8475–8505. doi: 10.1039/c2ee22310d
- Sun, F. M., Yan, C. F., Wang, Z. D., and Guo, C. Q. (2015). Ni/Ce-Zr-O catalyst for high CO<sub>2</sub> conversion during reverse water gas shift reaction (RWGSR). *Int. J. Hydrog. Energ.* 40, 15985–15993. doi: 10.1016/j.ijhydene.2015.10.004
- Sun, Q. D., Ye, J. Y., and Liu, C. J. (2014). In<sub>2</sub>O<sub>3</sub> as a promising catalyst for CO<sub>2</sub> utilization: a case study with reverse water gas shift over In<sub>2</sub>O<sub>3</sub>. *Greenhouse Gases* 4, 140–144. doi: 10.1002/ghg.1401
- Tang, Q. L., Hong, Q. J., and Liu, Z. P. (2009). CO<sub>2</sub> fixation into methanol at Cu/ZrO<sub>2</sub> interface from first principles kinetic Monte Carlo. *J. Catal.* 263, 114–122. doi: 10.1016/j.jcat.2009.01.017
- Ten Elshof, J. E., Bouwmeester, H. J. M., and Verweij, H. (1996). Oxygen transport through La<sub>1-x</sub>Sr<sub>x</sub>FeO<sub>3-δ</sub> membranes II. Permeation in air/CO, CO<sub>2</sub> gradients. *Solid State Ionics* 89, 81–92. doi: 10.1016/0167-2738(96)00255-X
- Tibiletti, D., Goguet, A., Meunier, F. C., Breen, J. P., and Burch, R. (2004). On the importance of steady-state isotopic techniques for the investigation of the mechanism of the reverse water-gas-shift reaction. *Chem. Commun.* 14, 1636–1637. doi: 10.1039/b403438d
- Utsis, N., Landau, M. V., Erenburg, A., Nehemya, R. V., and Hersowitz, M. (2018). Performance of reverse water gas shift on co-precipitated and carbon-templated BaFe-hexaaluminate effect of iron loading, texture, and promotion with Postassium. *ChemCatChem* 10, 3795–3805. doi: 10.1002/cctc.201800709
- Wang, C. C., and Nakamura, J. (2010). Structure sensitivity for forward and reverse water-gas shift reactions on copper structure surfaces: a DFT study. *J. Phys. Chem. Lett.* 1, 3053–3057. doi: 10.1021/jz101150w
- Wang, F., He, S., Chen, H., Wang, B., Zheng, L. R., Wei, M., et al. (2016b). Active site dependent reaction mechanism over Ru/CeO<sub>2</sub> catalyst toward CO<sub>2</sub> methanation. *J. Am. Chem. Soc.* 138, 6298–6305. doi: 10.1021/jacs.6b02762
- Wang, G. C., Jiang, L., Pang, X. Y., Cai, Z. S., Pan, Y. M., Zhao, X. Z., et al. (2003). A theoretical study of surface-structural sensitivity of the reverse water-gas shift reaction over Cu(hkl) surfaces. *Surf. Sci.* 543, 118–130. doi: 10.1016/S0039-6028(03)00876-8
- Wang, J. Y., Liu, C. Y., Senfile, T. P., Zhu, J., Zhang, G. H., Guo, X. W., et al. (2020). Variation in In<sub>2</sub>O<sub>3</sub> crystal phase alters catalytic performance toward the reverse water gas shift reaction. *ACS Catal.* 10, 3264–3273. doi: 10.1021/acscatal.9b04239
- Wang, L., Liu, H., Liu, Y., Chen, Y., and Yang, S. Q. (2013a). Effect of precipitants on Ni-CeO<sub>2</sub> catalysts prepared by a co-precipitation method for the reverse water-gas shift reaction. *J. Rare Earths* 31, 969–974. doi: 10.1016/S1002-0721(13)60014-9
- Wang, L. C., Khazaneh, M. T., Widmann, D., and Behm, R. J. (2013b). TAP reactor studies of the oxidizing capability of CO<sub>2</sub> on a Au/CeO<sub>2</sub> catalyst – A first step toward identifying a redox mechanism in the reverse water-gas shift reaction. *J. Catal.* 302, 20–30. doi: 10.1016/j.jcat.2013.02.021
- Wang, L. H., and Liu, H. (2018). Mesoporous Co-CeO<sub>2</sub> catalyst prepared by colloidal solution combustion method for reverse water-gas shift reaction. *Catal. Today* 316, 155–161. doi: 10.1016/j.cattod.2018.04.015
- Wang, L. H., Liu, H., Chen, Y., Zhang, R. K., and Yang, S. Q. (2013c). K-promoted Co-CeO<sub>2</sub> catalyst for reverse water-gas shift reaction. *Chem. Lett.* 42, 682–683. doi: 10.1246/cl.130137

- Wang, L. H., Liu, H., Liu, Y., Chen, Y., and Yang, S. Q. (2013d). Influence of preparation method on performance of Ni-CeO<sub>2</sub> catalysts for reverse water-gas shift reaction. *J. Rare Earths* 31, 559–564. doi: 10.1016/S1002-0721(12)60320-2
- Wang, W., Wang, S. P., Ma, X. B., and Gong, J. L. (2011). Recent advances in catalytic hydrogenation of carbon dioxide. *Chem. Soc. Rev.* 40, 3703–3727. doi: 10.1039/c1cs15008a
- Wang, W., Zhang, Y., Wang, Z. Y., Yan, J. M., Ge, Q. F., and Liu, C. J. (2016c). Reverse water gas shift over In<sub>2</sub>O<sub>3</sub>-CeO<sub>2</sub> catalysts. *Catal. Today* 259, 402–408. doi: 10.1016/j.cattod.2015.04.032
- Wang, X., Hong, Y. C., Shi, H., and Szanyi, J. (2016a). Kinetic modeling and transient DRIFTS-MS studies of CO<sub>2</sub> methanation over Ru/Al<sub>2</sub>O<sub>3</sub> catalysts. *J. Catal.* 343, 185–195. doi: 10.1016/j.jcat.2016.02.001
- Wang, X., Shi, H., Kwak, J. H., and Szanyi, J. (2015). Mechanism of CO<sub>2</sub> hydrogenation on Pd/Al<sub>2</sub>O<sub>3</sub> catalysts: Kinetics and transient DRIFTS-MS studies. *ACS Catal.* 5, 6337–6349. doi: 10.1021/acscatal.5b01464
- Wang, X., Shi, H., and Szanyi, J. (2017). Controlling selectivities in CO<sub>2</sub> reduction through mechanistic understanding. *Nat. Commun.* 8, 513–518. doi: 10.1038/s41467-017-00558-9
- Wang, Y. X., and Wang, G. C. (2019). A systematic theoretical study of water gas shift reaction on Cu(111) and Cu(110): potassium effect. *ACS Catal.* 9, 2261–2274. doi: 10.1021/acscatal.8b04427
- Weatherbee, G. D., and Bartholomew, C. H. (1984). Hydrogenation of CO<sub>2</sub> on group-VIII metals. 4. Specific activities and selectivities of silica-supported Co, Fe, and Ru. *J. Catal.* 87, 352–362. doi: 10.1016/0021-9517(84)90196-9
- Wenzel, M., Dharanipragada, V. R. A., Galvita, V. V., Poelman, H., Marin, G. B., Rihko-Struckmann, L., et al. (2017). CO product from CO<sub>2</sub> via reverse water-gas shift reaction performed in a chemical looping mode: Kinetics on modified iron oxide. *J. CO<sub>2</sub> Util.* 17, 60–68. doi: 10.1016/j.jcou.2016.10.015
- Wenzel, M., Rihko-struckmann, L., and Sundmacher, K. (2018). Continuous production of CO from CO<sub>2</sub> by RWGSR chemical looping in fixed and fluidized bed reactors. *Chem. Eng. J.* 336, 278–296. doi: 10.1016/j.cej.2017.12.031
- Wolf, A., Jess, A., and Kern, C. (2016). Syngas production via reverse water-gas shift reaction over a Ni/Al<sub>2</sub>O<sub>3</sub> catalyst: catalyst stability, reaction kinetics, and modelling. *Chem. Eng. Technol.* 39, 1040–1048. doi: 10.1002/ceat.201500548
- Wu, H. C., Chang, Y. C., Wu, J. H., Lin, J. H., Lin, I. K., and Chen, C. S. (2015). Methanation of CO<sub>2</sub> and reverse water gas shift reactions on Ni/SiO<sub>2</sub> catalysts: the influence of particle size on selectivity and reaction pathway. *Catal. Sci. Technol.* 5, 4154–4163. doi: 10.1039/C5CY00667H
- Wu, X.-F., Neumann, H., and Beller, M. (2011). Palladium-catalyzed carbonylative coupling reactions between Ar-X and carbon nucleophiles. *Chem. Soc. Rev.* 40, 4986–5009. doi: 10.1039/c1cs15109f
- Xu, H. C., and Ge, L. (2016). Progress on the catalytic hydrogenation of CO<sub>2</sub> via reverse water gas shift reaction. *Ind. Eng. Pro.* 35, 3180–3189. doi: 10.16085/j.issn.1000-6613.2016.10.023
- Yamazoe, N., Furukawa, S., Teraoka, Y., and Seiyama, T. (1982). The effect of oxygen sorption on the crystal structure of La<sub>1-x</sub>Sr<sub>x</sub>CoO<sub>3-δ</sub>. *Chem. Lett.* 10, 2019–2022. doi: 10.1246/cl.1982.2019
- Yamazoe, N., Teraoka, Y., and Seiyama, T. (1981). TPD and XPS study on thermal behavior of adsorbed oxygen in La<sub>1-x</sub>Sr<sub>x</sub>CoO<sub>3</sub>. *Chem. Lett.* 11, 1767–1770. doi: 10.1246/cl.1981.1767
- Yang, Q., and Lin, J. Y. S. (2006). Fixed-bed performance for production of oxygen-enriched carbon dioxide stream by perovskite-type ceramic sorbent. Separation and purification technology. *Sep. Purif. Technol.* 49, 27–35. doi: 10.1016/j.seppur.2005.08.004
- Yang, X. L., Su, X., Chen, X. D., Duan, H. M., Liang, B. L., Liu, Q. G., et al. (2017). Promotion effects of potassium on the activity and selectivity of Pt/zeolite catalysts for reverse water gas shift reaction. *Appl. Catal. B-Environ.* 216, 95–105. doi: 10.1016/j.apcatb.2017.05.067
- Yao, X. J., Tang, C. J., Ji, Z. Y., Dai, Y., Cao, Y., Gao, F., et al. (2013). Investigation of the physicochemical properties and catalytic activities of Ce<sub>0.67</sub>Mo<sub>0.33</sub>O<sub>2</sub> (M = Zr<sup>4+</sup>, Ti<sup>4+</sup>, Sn<sup>4+</sup>) solid solutions for NO removal by CO. *Catal. Sci. Technol.* 3, 688–698. doi: 10.1039/C2CY20610B
- Ye, J. Y., Liu, C. J., and Ge, Q. F. (2012). DFT study of CO<sub>2</sub> adsorption and hydrogenation on the In<sub>2</sub>O<sub>3</sub> surface. *J. Phys. Chem. C* 116, 7817–7825. doi: 10.1021/jp3004773
- Ye, J. Y., Liu, C. J., Mei, D. H., and Ge, Q. F. (2013). Active oxygen vacancy site for methanol synthesis from RWGSR on In<sub>2</sub>O<sub>3</sub> (110): a DFT study. *ACS Catal.* 3, 1293–1306. doi: 10.1021/cs400132a
- Yeung, C. M. Y., Yu, K. M. K., Fu, Q. J., Thompsett, D., Petch, M. I., and Tsang, S. C. (2005). Engineering Pt in ceria for a maximum metal-support interaction in catalysis. *J. Am. Chem. Soc.* 127, 18010–18011. doi: 10.1021/ja056102c
- Zhang, Q., and Guo, L. (2018). Mechanism of the reverse water-gas shift reaction catalyzed by Cu<sub>12</sub>TM bimetallic nanocluster: a density functional theory study. *J. Clust. Sci.* 29, 867–877. doi: 10.1007/s10876-018-1346-x
- Zhang, Q., Guo, L., and Hao, Z. J. (2018). Computational investigation of M<sub>1</sub>/W<sub>6</sub>S<sub>8</sub> (M=Fe, Ru, and Os) single-atom catalysts for CO<sub>2</sub> hydrogenation. *Catal. Surv. Asia* 22, 195–207. doi: 10.1007/s10563-018-9252-7
- Zhang, Q., Pastor-Pérez, L., Jin, W., Gu, S., and Reina, T. R. (2019b). Understanding the promoter effect of Cu and Cs over highly effective β-Mo<sub>2</sub>C catalysts for the reverse water-gas shift reaction. *Appl. Catal. B-Environ.* 244, 889–898. doi: 10.1016/j.apcatb.2018.12.023
- Zhang, X., Zhu, X. B., Lin, L. L., Yan, S. Y., Zhang, M. T., Liu, X., et al. (2016). Highly dispersed copper over β-Mo<sub>2</sub>C as an efficient and stable catalyst for the reverse water gas shift (RWGSR) reaction. *ACS Catal.* 7, 912–918. doi: 10.1021/acscatal.6b02991
- Zhang, Y., Liang, L., Chen, Z. Y., Wen, J. J., Zhong, W., Zou, S. B., et al. (2020). Highly efficient Cu/CeO<sub>2</sub>-hollow nanospheres catalyst for the reverse water-gas shift reaction: Investigation on the role of oxygen vacancies through in situ UV-Raman and DRIFTS. *Appl. Sur. Sci.* 516:146035. doi: 10.1016/j.apsusc.2020.146035
- Zhang, Z. M., Xun, H., Wang, Y., Hu, S., Xiang, J., Li, C. C., et al. (2019a). Regulation the reaction intermediates in methanation reactions vis modification of nickel catalysts with strong base. *Fuel* 237, 566–579. doi: 10.1016/j.fuel.2018.10.052
- Zheng, X. L., Guo, L., Li, W. L., Cao, Z. R., Liu, N. Y., Zhang, Q., et al. (2017). Insight into the mechanism of reverse water-gas shift reaction and ethanol formation catalyzed by Mo<sub>6</sub>S<sub>8</sub>-TM clusters. *Mol. Catal.* 439, 155–162. doi: 10.1016/j.mcat.2017.06.030
- Zheng, Z. Z., Xu, H. T., Xu, Z. L., and Ge, J. P. (2018). A monodispersed spherical Zr-based metal-organic framework catalyst, Pt/Au@Pd@UIO-66, comprising an Au@Pd core-shell encapsulated in a UIO-66 center and its highly selective RWGSR to produce CO. *Small* 14:1702812. doi: 10.1002/smll.201702812
- Zhou, G., Dai, B., Xie, H. M., Zhang, G. Z., Xiong, K., and Zheng, X. X. J. (2017). CeCu composite catalyst for CO synthesis by reverse water-gas shift reaction: effect of Ce/Cu mole ratio. *CO<sub>2</sub> Util.* 21, 292–301. doi: 10.1016/j.jcou.2017.07.004
- Zhou, G. L., Xie, F. Q., Deng, L. D., Zhang, G. Z., and Xie, H. M. (2020). Supported mesoporous Cu/CeO<sub>2-δ</sub> catalyst for CO<sub>2</sub> reverse water-gas shift reaction to syngas. *Int. J. Hydrog. Energy* 45, 11380–11393. doi: 10.1016/j.ijhydene.2020.02.058
- Zhou, K., and Li, Y. D. (2012). Catalysis based on nanocrystals with well-defined facets. *Angew. Chem. Int. Ed.* 51, 602–613. doi: 10.1002/anie.201102619
- Zhou, P., Ma, Y. C., Lan, G. J., Tang, H. D., Han, W. F., Liu, H. Z., et al. (2019). A highly stable and active mesoporous rethenium catalyst for ammonia synthesis prepared by a RhCl<sub>3</sub>/SiO<sub>2</sub>-templated approach. *Chinese J. Catal.* 40, 114–123. doi: 10.1016/S1872-2067(18)63192-4
- Zhuang, S. J., Han, N., Wang, T. T., Meng, X. X., Meng, B., Li, Y., et al. (2019). Enhanced CO selectivity for reverse water-gas shift reaction using Ti<sub>4</sub>O<sub>7</sub>-doped SrCe<sub>0.9</sub>Y<sub>0.1</sub>O<sub>3-δ</sub> hollow fibre membrane reaction. *Canad. J. Chem. Eng.* 97, 1619–1626. doi: 10.1002/cjce.23384
- Zonetti, P. C., Letichevsky, S., Gaspar, A. B., Sousa-Aguiar, E. F., and Appel, L. G. (2014). The Ni<sub>x</sub>Ce<sub>0.75</sub>Zr<sub>0.25-x</sub>O<sub>2</sub> solid solution and the RWGSR. *Appl. Catal. A-Gen.* 475, 48–54. doi: 10.1016/j.apcata.2014.01.004

**Conflict of Interest:** The authors declare that the research was conducted in the absence of any commercial or financial relationships that could be construed as a potential conflict of interest.

Copyright © 2020 Chen, Chen, Song, Ji, Wang, Wang and Cui. This is an open-access article distributed under the terms of the Creative Commons Attribution License (CC BY). The use, distribution or reproduction in other forums is permitted, provided the original author(s) and the copyright owner(s) are credited and that the original publication in this journal is cited, in accordance with accepted academic practice. No use, distribution or reproduction is permitted which does not comply with these terms.